Experiments in Fluids (2025) 66:114
https://doi.org/10.1007/s00348-025-04042-9

RESEARCH ARTICLE

How different are conventional and biofuel sprays applied to aviation? An infodynamic comparative analysis

Inês A. S. Ferrão[1,3,4] · Miguel R. O. Panão[2] · Miguel A. A. Mendes[3] · Ana S. H. O. Moita[4] · André R. R. Silva[1]

Received: 23 December 2024 / Revised: 21 April 2025 / Accepted: 22 April 2025
© The Author(s) 2025

Abstract

The transition from fossil to sustainable and alternative fuels is imperative to address environmental concerns and meet energy requirements. Thus, the implementation of alternative fuels requires a deeper investigation of spray behavior. This study explores conventional jet fuel (Jet A-1) and hydrotreated vegetable oil (HVO) in terms of breakup length and spray dynamics over a wide range of operating conditions. The normalized mean breakup length was measured, and an empirical correlation was developed based on the experimental data. Focusing on the droplet sizes in fuel sprays, which are critical for optimizing combustion, an informational perspective for comparative analysis was explored. The terms informature, infotropy, and infosensor were introduced to quantify and capture the non-deterministic nature of physical systems. The results revealed similar drop size distributions for HVO and Jet A-1, with the Gamma function effectively characterizing the distributions. Both fuels exhibit spray evolution toward higher complexity states, emphasizing the role of aerodynamic forces and minimum development distance in atomization. The new lexicon of infodynamics views sprays as networks of information flow, with infotropy indicating that both fuels produce sprays with similar degrees of transformation. HVO is endorsed as a viable alternative with broader implications for sustainable aviation solutions and understanding complex engineering processes.

List of symbols

a, b	Scale and shape parameters in probability distributions
C, C_n	Complexity [nats^2] and normalized by the maximum informature
D	Drop size [μm]
D_{50}	Median drop diameter [μm]
f	Frequency probability of a distribution
F	Cumulative frequency of a distribution
H_b	Infotropy of a non-deterministic physical system [a.u.]
H_δ	Analytical differential informature [a.u.]
H_Δ	Discrete differential informature [a.u.]
H_I	Informature [a.u.]
$H_{\max,b}$	Maximum informature [a.u.]
H_n	Normalized informature
K_b	Logarithm-base conversion constant
K_c	Arbitrary contextual scale of an infotropy
$\dot{m}$	Mass flowrate [g/s]
M	Momentum flux ratio
$nH_{ud,b}$	Mutual informature between velocity u and size d [nats]
Oh	Ohnesorge number
p	Probability density [μm^{-1}]
R_n	Normalized redundancy
s	Log-normal standard deviation [μm]

Inês A. S. Ferrão, Miguel R. O. Panão, Miguel A. A. Mendes, Ana S. H. O. Moita and André R. R. Silva have contributed equally to this work.

✉ Inês A. S. Ferrão
ines.ferrao@ubi.pt

Miguel R. O. Panão
miguel.panao@dem.uc.pt

Miguel A. A. Mendes
miguel.mendes@tecnico.ulisboa.pt

Ana S. H. O. Moita
anamoita@tecnico.ulisboa.pt

André R. R. Silva
andre@ubi.pt

[1] Universidade da Beira Interior, AEROG, LAETA, Covilhã, Portugal

[2] Universidade de Coimbra, ADAI, LAETA, Coimbra, Portugal

[3] Instituto Superior Técnico, Universidade de Lisboa, IDMEC, LAETA, Lisboa, Portugal

[4] Instituto Superior Técnico, Universidade de Lisboa, IN+, LARSyS, Lisboa, Portugal

Published online: 27 May 2025

u_d	Drop velocity [m/s]
We_d	Weber number

Subscripts

0	Initial event
a	Air, aerodynamic
b	Logarithm base
d	Droplet
$d50$	Median representative quantity
e	Exponential base
f	Fuel

Greek symbols

Δt	Total measurement time [s]
κ	Contextual infodynamic parameter [a.u.]
ρ	Density [kg/m^3]
σ	Surface tension [N/m]
τ	Infosensor response time [s]

Abbreviations

AFR	Air–fuel ratio [−]
HVO	Hydrotreated vegetable oil
KS	Kolmogorov–Smirnov
LN	Log-normal
PDF	Probability density function
SMD	Sauter mean diameter

1 Introduction

Climate change is a global phenomenon, and it is essential to address it urgently to protect living beings and ecosystems. The longer we wait, the more difficult it becomes to solve the problem. The leading causes of climate change are heavily reliant on industrial and non-renewable energy sources. In addition, political actions have been taken to ensure a global energy economy, supply, and security. In 2015, the Paris Agreement focused on restricting the global temperature increase to below 2 °C above the pre-industrial level and efforts to restrict it to 1.5 °C (Cabrera and Sousa 2022). Its purpose is to achieve net carbon neutrality by 2050 while ensuring energy requirements. According to Scott and Lindsey (2016), human activities are responsible for emitting 60 or more times the amount of carbon dioxide released by volcanoes each year. However, energy systems in developing nations rely heavily on fossil fuels, which are non-renewable energy sources (Yang et al. 2023). In particular, the transportation sector relies on petroleum fuels, which account for approximately 19% of the global energy usage and contribute to approximately 23% of greenhouse gas emissions (Ershov et al. 2023). The primary fuel source for the transportation sector is liquid fuels provided by petroleum, owing to their high energy density, ease of transport and storage, and extensive global infrastructure established over the past century to maintain this system (Khan et al. 2023).

Therefore, it is imperative to explore sustainable and alternative energy sources to mitigate these environmental issues. In this context, air transportation has focused on the energy transition associated with the reduction in greenhouse gas and pollutant emissions. Aviation primarily relies on a limited supply of fossil fuels, known as jet fuel, which significantly contributes to air pollution. To change this perspective, sustainable aviation fuel (SAF) has been investigated and introduced in this industry. Several alternatives have been discussed, primarily focusing on drop-in biofuels, batteries, hydrogen, and fuel cells (Afonso et al. 2023).

The International Air Transport Association (IATA) has recognized that drop-in biofuel is the most favorable strategy, particularly in the short term, to mitigate the environmental impact of the aviation sector (Cabrera and Sousa 2022). Drop-in biofuels generally refer to fuels derived from biomass sources and renewable feedstocks acquired using biological, thermal, and chemical conversion methods (Afonso et al. 2023). Drop-in fuels are related to a direct replacement or blend for conventional jet fuel (typically Jet A or Jet A-1) without demanding any aircraft engine or fuel infrastructure modification (Okolie et al. 2023). Biofuels are crucial for achieving carbon neutrality because plants absorb CO_2 during biomass growth, which is practically identical to the amount of carbon dioxide released into the atmosphere by combustion processes in aero-engines (Khan et al. 2021). A mixture of jet fuel and biofuel has already been tested, and favorable findings have been reported. Current legislation permits certified SAF to be blended to a maximum ratio of 50% with fossil-based jet fuel, depending on the feedstock production pathway considered.

In the SAF pathway, the HEFA (Hydroprocessed Esters and Fatty Acids) conversion process is a fully commercialized and mature technology that already operates in aviation gas turbines (Abrantes et al. 2021). In addition to these advantages, biofuels can possess unique properties that affect the atomization process, depending on the feedstock production pathway, influencing combustion performance and emissions. It is essential to ensure that the fuel is atomized efficiently to achieve optimal combustion. Poor atomization can lead to larger droplets, resulting in localized fuel-rich combustion. This process can produce soot and nitric oxide in combustion systems, as reported by Chong and Hochgreb (2015). Therefore, a thorough understanding of spray dynamics is necessary for developing combustion chambers and injection systems. These dynamics consist of a first stage of primary atomization with the formation of ligaments that disintegrate into droplets and a second stage concerning spray development and propagation. To assess whether biofuels can replace conventional fossil fuels, it is essential to identify the challenges associated with the

atomization dynamics during both primary and secondary atomization stages, as well as the combustion characteristics of biofuels.

1.1 Primary atomization challenge

Atomization can be used in many applications, from medicine to agriculture, and more specifically, in gas turbines, industrial furnaces, and rocket engines. This process is defined as the conversion of a bulk liquid into a dispersion of small droplets from submicron to several hundred microns in diameter (Lefebvre and McDonell 2017). Disintegration into small droplets occurs when the disruptive forces surpass the liquid surface tension forces. Typically, atomizers or spray nozzles provide sufficient energy to the liquid flow and generate instabilities that result in jet liquid fragmentation. Two examples of atomizers are pressure and twin-fluid atomizers, where the former is related to the discharge of liquid at high speed into quiescent or relatively slow-moving gas. In contrast, twin-fluid atomizers operate with a relatively slow-moving liquid to a high-velocity airstream, require lower fuel pressures, and produce a finer spray suitable for cold and viscous fuels (Mao 1987; Lefebvre 1980). Twin-fluid atomizers can be classified as air-assist or airblast atomizers, depending on the amount of air supplied to the atomizer. The performance of an atomizer depends on the nozzle geometry, operating conditions, and physical properties of the dispersed and continuous phases (Roudini and Wozniak 2018; Lefebvre and McDonell 2017).

Atomization has attracted the scientific community over the last century, providing valuable theoretical and experimental investigations. In this respect, spray formation can be classified into two phases. The first phase, or initial disintegration, is denominated by primary atomization and is characterized by the disintegration of a liquid jet into ligaments or fragments. When a liquid jet is released from the nozzle as a continuous cylindrical body, oscillations and perturbations emerge because of the imbalance between cohesive and disruptive forces on its surface. When amplified under specific conditions, these oscillations fragment the jet into droplets. During this process, bag-like structures and ligaments are observed. In contrast, secondary atomization involves disintegration into smaller droplets. If the larger droplets produced during the primary atomization are subjected to an ambient flow field moving at a relative velocity, aerodynamic forces may induce deformation, resulting in their fragmentation into smaller droplets, evidencing secondary atomization. Typically, primary atomization occurs near the nozzle, and secondary atomization occurs downstream (Roudini and Wozniak 2018).

To comprehensively understand the primary breakup mechanism, the behavior of cylindrical liquid jets discharged into a quiescent environment should be addressed. Furthermore, liquid jet breakup can be classified into five regimes: dripping, Rayleigh, first wind-induced, second wind-induced, and atomization regimes. The transition between regimes can also be determined by using the corresponding Weber numbers. The Weber number (We) is the ratio between the inertial (or aerodynamic) and surface tension forces and can be expressed by the following expression:

$$We = \frac{\rho U_l^2 L}{\sigma}, \tag{1}$$

where ρ is the liquid density, σ is the surface tension, U_l is the velocity of the liquid jet, and L is the characteristic length of the liquid flow, more concretely, the jet diameter. In the dripping regime, owing to the significantly low outlet velocity, liquid accumulates at the nozzle tip until it eventually detaches and drips. The Rayleigh regime is associated with the formation of droplets with uniform sizes greater than the nozzle outlet diameter when the air velocity is considerably low. Consequently, by increasing the air velocity, the influence of aerodynamic force on jet breakup becomes relevant (Kumar and Sahu 2019). In the first wind-induced regime, droplets were formed at a considerable distance from the nozzle exit and exhibited diameters comparable to the nozzle outlet diameter. In the second wind-induced regime, atomization was enhanced, resulting in reduced breakup lengths and smaller droplet diameters. The atomization regime corresponds to a droplet diameter that is significantly smaller than the nozzle diameter (Reitz and Bracco 1982; Payri et al. 2011). Table 1 shows the boundaries of each regime, defined by the Weber number presented in Eq. (1) and the gas Weber and Ohnesorge numbers. The latter dimensionless number represents the ratio of the internal viscous force to the surface force resulting from the surface tension.

$$Oh = \frac{\mu}{\sqrt{\rho \sigma L}}, \tag{2}$$

where μ is the liquid dynamic viscosity, σ is the surface tension, ρ is the liquid density, and L is the characteristic length. Thus, the Weber number of gas is defined as follows:

Table 1 Regime map of a liquid jet breakup discharged into a quiescent environment, adapted from Miesse (1955); Chigier (1996); Lin and Reitz (1998); Dumouchel (2008)

Regimes	Criteria
Dripping regime	$We < 8$
Rayleigh regime	$We > 8\, We_g < 0.4$ or $1.2 + 3.41 Oh^{0.9}$
First wind-induced regime	$1.2 + 3.41 Oh^{0.9} < We_g < 13$
Second wind-induced regime	$13 < We_g < 40.3$
Atomization regime	$We_g > 40.3$

$$We_g = \frac{\rho_g U_l^2 L}{\sigma}, \tag{3}$$

ρ_g is the density of the gas, σ is the surface tension, U_l is the velocity of the liquid jet, and L is the characteristic length of the liquid flow, or more concretely, of the jet diameter.

In combustion systems, liquid fuels are atomized before the combustion process, producing small droplets that allow a higher surface area, reduce the vaporization time, and lead to better air-to-fuel mixing, significantly impacting combustion emissions, performance, and flame stability. Because liquid atomization is crucial for engine performance and subsequent emissions, investigations focused on comparing alternative and conventional fuels are vital to advancing the implementation of sustainable fuels in the modern world. As previously noted, as the fuel exits the nozzle, turbulence and the aerodynamic interaction of the fuel and air promote instability of the jet and result in ligaments and droplets near the nozzle. This highlights the non-deterministic nature of primary atomization, which subsequently breaks into smaller ones, affecting the ignition behavior, heat release, fuel consumption, and exhaust emissions of the combustion reaction. Consequently, understanding the physical phenomena of primary atomization plays a relevant role in determining the connection between nozzle design and the diversity of droplet sizes produced, which requires further investigation (Esposito 2019; Vijay et al. 2015). In this context, studies on the breakup length can provide valuable insights into the atomization quality. Several authors have proposed correlations as functions of dimensionless numbers to predict and understand the breakup length, as listed in Table 2. These correlations are related to the mean breakup length and are mainly obtained through shadowgraph measurements. A detailed review dedicated to primary atomization, in particular, to air-assisted atomization, was performed by Dumouchel (2008).

The liquid Reynolds Number (Re_L) considered for breakup length analysis can be defined by the following expressions:

$$Re_L = \frac{U_L D_L}{\nu_L} \tag{4}$$

where U_L is the liquid velocity, D_L is the bore liquid diameter, and ν_L is the liquid kinematic viscosity. The aerodynamic Weber Number (We_a) presented in Table 2 is based on relative velocity and is defined by the following expression:

$$We_a = \frac{\rho_a (U_a - U_L)^2 D_L}{\sigma}, \tag{5}$$

where U_a is the air velocity and σ is the liquid surface tension. The momentum flux (M) was also investigated in accordance with the findings of Lasheras and Hopfinger (Lasheras 2000), who stated that it represents the most pertinent parameter for assessing the breakup of an unbroken liquid core. The momentum flux ratio (M) is represented by

$$M = \frac{\rho_a U_a^2}{\rho_L U_L^2}, \tag{6}$$

In addition to the studies that provided breakup length correlations, Sikka et al. (2021) evaluated primary atomization, stating that an increase in the air-to-liquid momentum relation leads to the dominance of aerodynamic effects (e.g., a swirl flow field); consequently, a reduction in the liquid core length. Thus, the breakup length is inversely proportional to AFR (air–fuel ratio). This outcome improves the fuel–air mixing and promotes vaporization, thereby stabilizing the combustion of liquid fuel (Soni and Kolhe 2021).

1.2 Spray development challenge

Following the earlier discussion, exploring alternative and sustainable solutions to address environmental concerns in the aviation sector is fundamental. From this perspective, within complexity science, the present study introduces an infodynamic comparative analysis to investigate the differences between alternative and conventional fuel sprays. In conventional data analysis of spray characteristics, the focus is on the average droplet sizes and velocities, from which one determines the dimensionless numbers relating several forces and energy components involved in liquid atomization. However, because of its reductionist nature, once the analysis proceeds with average quantities, all the information contained in the distributions is no longer part of the analysis. Figure 1, produced by simulating typical drop distributions in spray, illustrates the distinction between the drop statistics expressed through the known Sauter mean diameter

Table 2 Correlations for the characteristic length of air-assisted/airblast atomization

Authors	Correlations	Re_L	We_a	M
Eroglu et al. (1991)	$\overline{L}/D_L = 0.66 We_a Re_L^{0.6}$	1100–18000	13–267	
Leroux et al. (2007)	$\overline{L}/D_L = 10 M^{-0.3}$	45–1000	1–1000	0.17–60
Zhao et al. (2014)	$\overline{L}/D_L = 5.2(\frac{A_L}{A_a})^{-0.17} M^{-0.28}$	783–35000	8.8–455	0.011–620
Kumar and Sahu (2018)	$\overline{L}/D_L = 5.45 M^{-0.22}$	3000–5000	80–300	1.1−8.3

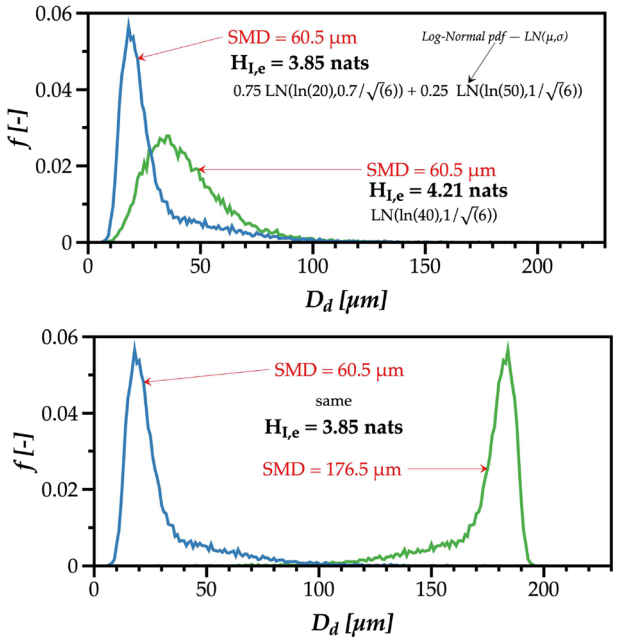

Fig. 1 Example of distinction between drop statistics and infodynamic analysis

(SMD) and an infodynamic parameter defined in Sect. 3, which quantifies the amount of information in *nats* ("natural units") of a frequency probability distribution (*f*) of drop sizes. On the left, the SMD is blind to the distribution of drop sizes, and different distributions can result in the same SMD. However, on the right, if one mirrors the frequency probabilities relative to size classes, the amount of information is blind to the position of the frequency probabilities but not the SMD. Therefore, a counterposition between conventional drop statistics and infodynamic analysis is misleading because these methods address different levels of spray data interpretation.

One frequently reads how sprays are complex flows, but little has been done to quantify this complexity, rooted in the amount of information on the spray. An infodynamic analysis represents a step forward in the quantification and understanding of the non-deterministic nature and complexity of liquid atomization and spray dynamics from the perspective of its information content.

Based on the literature and the importance of evaluating alternative fuels for aviation purposes, the present study was dedicated to visualizing and understanding near-nozzle breakup. The breakup length will be explored under a wide range of operating conditions, and a correlation is presented in accordance with the experimental data. In addition, the mathematical nature of the drop size distributions of conventional and alternative aviation fuels using infodynamics will be addressed, and an analysis will be provided to measure the spray complexity and infodynamic properties.

Table 3 Jet A-1 and HVO properties (Ferrao et al. 2021)

Parameter	Jet A-1	HVO
Density (Kg/m^3) (at 20 °C)	789	780.6
Surface Tension (mN/m) (at 20 °C)	24.7	26.5
Kinematic Viscosity (mm^2/s (at 25 °C)	1.40	4.33
Sulfur (wt.%)	0.3	0.09
Aromatics (wt.%)	13.8	0
Flash Point (°C)	38	99
Final Boiling Point (°C)	237	308
Cloud Point (°C)	− 26	− 30
Lower Heating Value (MJ/kg)	43	43.9
Higher Heating Value (MJ/kg)	47	47.1
Distillation 10 vol. % (°C)	170	262
Hydrogen Content	14.5	15.4
Carbon Content	84.6	85.5
H/C Ratio	1.91	2.18

2 Experimental setup and diagnostic technique

The present section presents the experimental setup and laser diagnostic technique and describes the image data processing employed. In this study, conventional and alternative jet fuels were compared. Jet A-1 is a liquid fuel derived from kerosene and designed for applications in the aeronautical industry. For aviation purposes, Jet A-1 is enriched with several additives that aim to inhibit the hazard of static charges, reducing the oxidizing and corrosive potentials while increasing lubricity and improving cold flow properties (Chuck 2014). Moreover, aero-engines must be powered by fuels with high energy content, good flow characteristics, thermal stability, and restrictions to ensure reliability, safety, and security (Blakey et al. 2011). The alternative jet fuel used in this study was NEXBTL (HVO) acquired from NESTE. This liquid biofuel is obtained by converting vegetable oils and animal fats into paraffinic hydrocarbons. HVO presents acceptable cold flow properties, high cetane number, reasonable distillation range, and high thermal stability. It is free of aromatics and sulfur. Additionally, it presents stable storage resistance to microbial growth, thereby avoiding the formation of engine deposits. According to the literature, the use of HVO has shown advantages in reducing greenhouse gases and pollutant emissions (Pinto et al. 2023; Mikkonen et al. 2013; Aatola et al. 2008). Table 3 shows the properties of Jet A-1 and HVO fuels.

Figure 2 schematically represents the experimental setup used to characterize the spray. For the spray visualization tests, an air-assisted SCHLICK Two-Substance Nozzle Model 0/2 atomizer with external mixing and swirl grooves was used. The vanes present in the airstream line promote swirl, thereby improving the mixing of air and fuel droplets

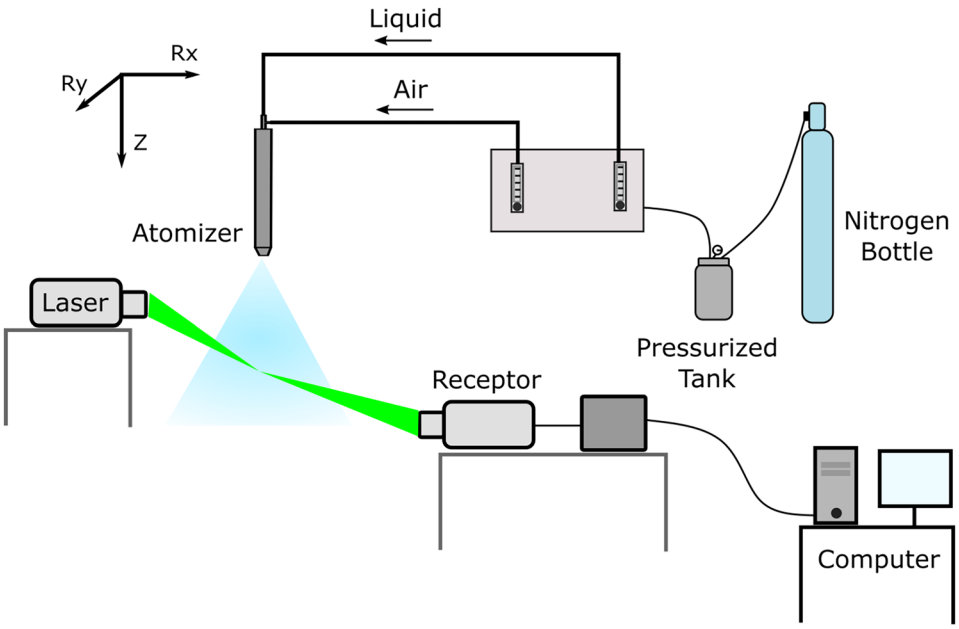

Fig. 2 Experimental setup: phase Doppler interferometry

(Beck et al. 1991). The atomizer was placed vertically downward to avoid overlapping droplets during recirculation. The liquid fuel and air atomization flowrates were controlled by two different rotameters: ABB PurgeMaster. A maximum volumetric capacity of 1.15 L/h was used for the fuel rotameter. A rotameter with a capacity of 54 L/min was used for the air atomization. For Jet A-1 and HVO, the same rotameter was used to control the flowrate.

Consequently, a calibration was required to assess the effective flowrate dispensed by the atomizer, as previously described in Ferrão et al. (2024). The theoretical flowrate is related to the volumetric flowrate released by the rotameter. However, when a specific theoretical flowrate is imposed, the fuel flowrate release departs from the expected value. The effective flowrate was evaluated, corresponding to the volumetric flowrate of the fuel released by the flowmeter. This analysis was carried out three times for each fuel and flowrate condition, with each examination lasting two to three minutes, resulting in a maximum standard deviation of 0.0028 L/h.

The air–fuel ratio (AFR) corresponds to the mass flowrate ratio of air ($\dot{m}_a$) and fuel ($\dot{m}_f$), which is expressed as

$$\mathrm{AFR} = \frac{\dot{m}_a}{\dot{m}_f} \tag{7}$$

Table 4 lists the operating conditions in terms of the air flowrate and air–fuel ratio (AFR), as well as the corresponding dimensionless numbers defined in Sect. 1.

The delivery of liquid fuel is performed with the aid of a pressure tank at 1 bar. Additionally, a nitrogen bottle was used to pressurize the fuel tank at 1 bar; subsequently, a manually regulated valve was used to regulate the fuel that passed through the rotameter to feed the atomizer. The air flowing to the atomizer was pressurized by a compressor to a value of 2 bar and regulated by a manual valve. With respect to the operating conditions, liquid and air interactions occur under ambient and atmospheric conditions. The atomizer has free movement in Rx, Ry, and Z, which allows it to change its position. Phase Doppler measurements were performed at axial locations of $Z = 5$, 10, 15, and 20 mm from the atomizer exit, $Z = 0$ mm. The selection of these distances is correlated with the breakup structure of the spray. For each Z, a set of measurements was performed along the radial x-y axes in 2 mm steps for the two perpendicular axes. Droplet size and velocity distributions were measured using a phase Doppler interferometry system (FlowExplorer 1D transmitting and receiving optics connected to a BSA F100 processor from Dantec Dynamics). The system was used for transmitting an optical laser power of 90 mW for the axial velocity (U) component measurements, with a wavelength of 660 nm. The focal length was 500 mm, and the beam spacing was 37 mm. The receiving optics was a fiber PDI with a receiver focal length of 400 mm. The scattering angle is 31°. Table 5 summarizes the PDI measurement configuration.

2.1 Image data processing

Obtaining quantitative measurements from image acquisition requires image data processing, which is essential for ensuring that the imaging technique can provide reliable and consistent measurements. An imaging technique was applied to different fuels and air–fuel ratios to provide data images. The images should be carefully treated to perform detailed

Table 4 Jet A-1 and HVO operating conditions and the corresponding dimensionless numbers

Fuel conditions	$\dot{m}_a$(g/s)	Jet A-1				HVO			
		Re_L	We_a	M	AFR	Re_L	We_a	M	AFR
1stCondition	0.11	61.0	1.6	5.6	2.6	19.1	1.5	6.0	2.7
	0.22	61.0	6.6	22.5	5.2	19.1	6.1	24.2	5.4
	0.33	61.0	15.0	50.7	7.9	19.1	13.8	54.4	8.1
	0.66	61.0	60.1	202.9	15.7	19.1	55.6	217.8	16.2
2ndCondition	0.11	72.2	1.6	4.0	2.2	22.8	1.5	4.2	2.3
	0.22	72.2	6.6	16.1	4.4	22.8	6.1	4.1	4.5
3rdCondition	0.11	92.4	1.6	2.5	1.7	29.8	1.5	2.5	1.7
	0.22	92.4	6.6	9.8	3.5	29.8	6.1	9.9	3.5
4thCondition	0.11	122.8	1.6	1.4	1.3	39.2	1.5	1.4	1.3
	0.22	122.8	6.5	5.6	2.6	39.2	6.0	5.8	2.6
	0.33	122.8	14.8	12.5	3.9	39.2	13.7	13.0	3.9
	0.55	122.8	59.8	50.0	7.8	39.2	55.3	51.9	7.9
5thCondition	0.11	144.4	1.6	1.0	1.1	55.0	1.4	0.7	0.9
	0.22	144.4	6.5	4.0	2.2	55.0	5.9	2.9	1.9

Table 5 PDI measurement configuration

Beam system	U1
Transmitting Optics	
Laser power	90 mW
Wavelength	660 nm
Focal length	500 mm
Beam spacing	37 mm
Receiving Optics	
Receiver Type	Fiber PDI
Scattering angle	31°
Receiver focal length	400 mm
Software Parameters	
Photomultiplier Sensitivity	900 V
Signal Gain	16 dB
Center Velocity	−16.34 m/s
Velocity Span	43.03 m/s

measurements of the spray characteristics. Measuring the breakup length is challenging; therefore, several images were recorded in the focus structures for further analysis. To accomplish this, an algorithm was developed using MATLAB software (Inc 2022). An illustration of the algorithm dedicated to breakup length measurements is shown in Fig. 3. A series of actions were performed to acquire the breakup length of each fuel, requiring instantaneous breakup length images and background images, as shown in Fig. 4. The first step is to subtract the background and instantaneous breakup length images. Then, the subtracted image is applied and binarized through a threshold value selected based on meticulous analysis, as shown in Fig. 4b.

The images were cropped to highlight the spray structure. The breakup length corresponding to the continuous fluid structure was identified, and its dimensions were determined by a function denoted as "region props." In this context, the breakup length represents the maximum extent along the axial direction, identified as the structure with the highest area. Moreover, the position of the region box was analyzed to ensure that the measurements were only focused on the continuous portion of the jet, measured from the nozzle to the breakup point. If the analyzed region was not connected to the nozzle, the image was discarded, and a novel image was investigated. All the data related to the height, width, and position of the breakup structure were exported to a matrix for further evaluation. In this analysis, the evaluated data correspond to a continuous liquid portion attached to the atomizer nozzle, and any secondary droplets are discarded, as shown in Fig. 4c. This study also provides an investigation dedicated to an analysis of the droplet diameter originating from the filament and rim disintegration that appears downstream of the nozzle, as shown in Fig. 4. To achieve this objective, the breakup length algorithm was adapted. In this respect, the background and instantaneous images were subtracted and binarized using the threshold previously employed for the breakup length measurements. After this, the "region props" function was applied to determine elements with an eccentricity equal to or higher than 0.6. This parameter was considered in order to capture the droplet's circular shape, and this eccentricity value was determined based on the analysis to exclude any elongated filaments present in the images. When the selection of the droplets is completed, the algorithm extracts their diameter based on the droplet area. For each image, a set of data on droplet diameter is provided. Hence, identical droplets between frames were excluded from the analysis. The pixel sizes were 0.035 and 0.031 mm/pixel for Jet A-1 and HVO, respectively.

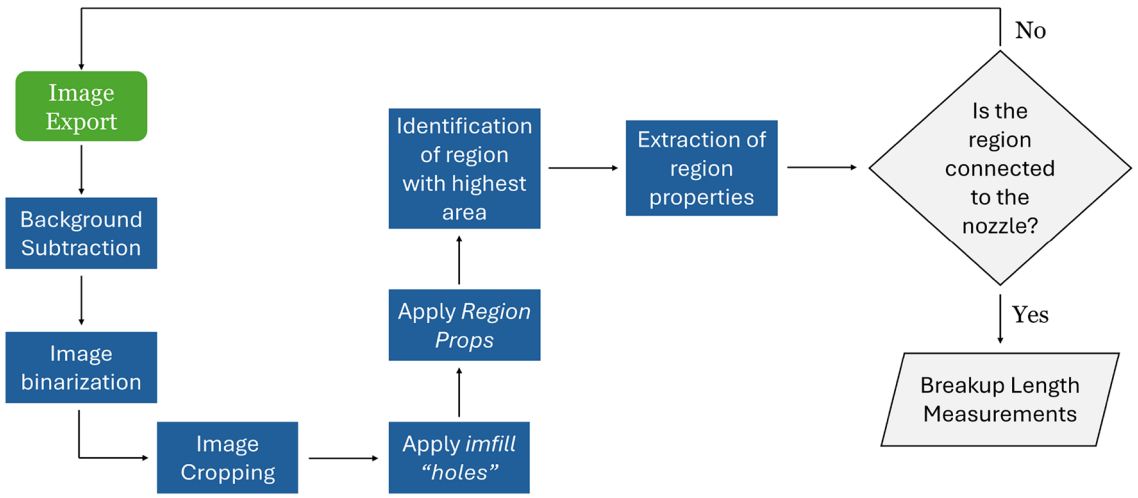

Fig. 3 Illustration of the image data processing for breakup length

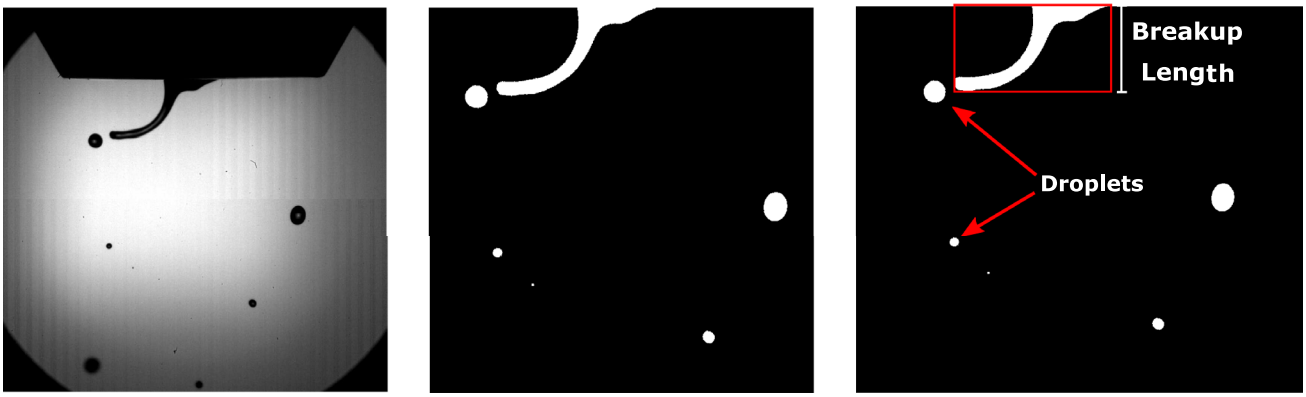

Fig. 4 Image data processing for breakup length: **a** Original image; **b** Cropped image; and **c** Identification of the breakup length

3 Infodynamic analysis fundamentals

Panão (2025) has recently introduced the fundamentals of an infodynamic analysis adapted to engineering. This section summarizes the main ideas.

When Claude Shannon (1948) deduced his formulation for the amount of information produced by a process affected by randomness owing to its nature or the influence of noise, he expressed it as a *"measure of information, choice and uncertainty"* (see Shannon (1949), p. 50).

$$H = -K \sum_i f_i \log_2(f_i) \tag{8}$$

where K is an arbitrary constant and f_i is the probability (frequency) of the occurrence of x_i, $\sum_i f_i = 1$. This parameter has all the characteristics of an uncertainty (Shannon 1949), and according to Tribus and McIrvine (1971), K determines the unit of information and usually takes the form of ln(2) to change the logarithm base to e. However, the most common terminology for H is *Shannon entropy*, owing to its similarity with the Boltzmann H-theorem function. In addition, Tribus and McIrvine (1971) revealed that Shannon's designation of his formulation as an "entropy" was suggested by John von Neumann. However, Denbigh (1981) argued that this suggestion is a disservice to Shannon's work because functions with the same formal structure do not necessarily represent the same. To overcome this misleading designation, two neologisms are introduced: *informature* and *infotropy*. Also, the following subsection shows their relation to complexity.

3.1 Informature, infotropy, and complexity

Informature is the block in Shannon's formulation that measures the amount of information from the knowledge of the probability distribution,

$$H_{I,b} = -K_b \sum_i f_i \log_2(f_i) \tag{9}$$

where K_b is the first part of $K = K_b \cdot K_c$, which establishes the logarithmic base; therefore, if $K_b = \log_2(2) = 1$, the logarithm is the original base-2 of Shannon's formulation, and the *informature* is in "binary units" or *bits*. If $K_b = \ln(2)$, the base changes to the natural logarithm, and the *informature* is in "natural units" or *nats*. One should consider *informature* measurements of the amount of information in a stochastic system in *bits* or *nats*, similarly to considering temperature measurements in Kelvin or mass measurements in grams. The *informature* is an extensive property because it depends on the number of categories describing the non-deterministic nature of the physical system.

In Shannon's formula, the second part of K, K_c, contextualizes the informature, leading to the second neologism of *infotropy*, synthesizing "information" (*info-*) and transformation (from the Greek *trope*, as in Clausius's invention of the word "entropy"). For example, when $K_c = k_B$ (Boltzmann's constant), $K_b = \ln(2)$, and $f_i = 1/W$ is constant, W corresponding to the number of microstates in a gaseous system, $H_e = S = k_B \ln(W)$, which is Boltzmann's formula for the thermodynamic entropy, a gaseous *infotropy* where Boltzmann's constant contextualizes the maximum *informature* obtained for a fully chaotic physical system, such as a gas at a microscopic level in Boltzmann's perspective. These neologisms overcome the shortcomings of Neumann's suggestion and avoid mistaking Shannon's measure of information for a concept similar to that of thermodynamic entropy. Thus, one rewrites Shannon's *infotropy* as

$$H_b = K_c \times H_{I,b} \tag{10}$$

In the new terminology, H in Eq. (8) is H_2 because Shannon applies a base-2 logarithm. When applying *infotropy* to a continuous function, because it is an extensive property, it means $H_b \to \infty$. Therefore, Stone (2015) explains how one can ignore this infinity by considering the differential part of the measure of information, $H_{\Delta,e}$. In discrete probability distributions, the differential *informature* is given by

$$H_{\Delta,e}[nats] = -\sum_{i=1}^{N_k} f_i \ln(p_i) \tag{11}$$

where N_k is the number of classes and $p_i = f_i/\Delta x_i$ is the probability density dividing the frequency of a class (f_i) by its size (Δx_i). In this case, unlike the *informature* defined in Eq. (9), this measurement becomes an intensive property of the system because it depends on the size of classes defined for the system. For a continuous function, the differential *informature* adapted to drop size distributions corresponds to

$$H_{\delta,e} = \int_0^\infty p(x) \ln\left(\frac{1}{p(x)}\right) dx \tag{12}$$

According to Stone (2015), as the number of classes increases, $H_{\Delta,e} \to H_{\delta,e}$, which is the basis of the approach followed in this study. The third and final concept is statistical complexity. Consider the relative information, also known as the Kullback–Leibler information distance or information gain. It measures the distance between the maximum informature, $H_{max,b} = K_b \cdot \log_2(N_k)$, where all possible configurations (N_k) are equally probable, and the actual informature given by Eq. (9),

$$D = H_{\max,b} - H_{I,b} \tag{13}$$

According to Feldman and Crutchfield (1998), one can quantify the statistical complexity of a finite-size system as the product between its informature and the relative information as

$$C = H_{I,b} \times D \tag{14}$$

Systems without information ($H_{I,b} = 0$) have no complexity ($C = 0$), as well as fully indeterminate systems ($D = 0$). However, if one divides the complexity by the square of the maximum informature, this quantity becomes dimensionless

$$C_n = H_n \cdot R_n \tag{15}$$

where $H_n = H_{I,b}/H_{max,b}$, and $R_n = \left(1 - H_n\right)$ correspond to the redundancy, which measures the likelihood of structures being present in the spray information. Suppose that there is only one mechanism leading to droplets of a single size. In this case, the polydispersion degree (how many different sizes are relevant in the spray) is low, implying regularity in the atomization mechanisms, leading to a well-defined spray structure with droplets of regular sizes. In contrast, if more than one physical process atomizes the liquid, for example, a combination of aerodynamic forces of an air-assisted jet, stretching of ligaments, and bag breakup, the multitude of physical mechanisms leads to a less structured spray with lower redundancy.

What exactly is the statistical complexity measuring? Statistical complexity measures the degree of spray organization. This is the combined effect of the

- The non-deterministic part associated with the polydispersion degree of drop size diversity (see Panão et al. (2020)) expressed by the normalized informature (H_n);

- And the deterministic part associated with the degree of structure expressed by redundancy, given by the hydrodynamic morphology of instabilities or a certain dispersion pattern resulting from the interaction between droplets and the environment, implying a diversity of physical mechanisms spatiotemporally organizing the spray propagation.

A highly complex spray is not an unexplainable spray unless we do it empirically, but it is formed and developed with a proper balance between the diversity of drop characteristics and the physical mechanisms structuring the spray development. In the context of the drop size distribution of a spray, a high C_n value indicates a distribution that is both diverse and structured, suggesting a well-organized system with moderate indeterminacy. Conversely, a low C_n value suggests either a fully controlled atomization with low indeterminacy and well-defined atomization mechanisms or a fully uncontrolled atomization with high indeterminacy and a multitude of physical mechanisms structuring the spray. Both indicate lower organizational levels of drop dispersion. Thus, C_n serves as a useful metric for evaluating the organization of droplet distributions in various engineering physical systems containing deterministic and non-deterministic elements.

How should one use complexity measure? What questions might it help answer? The statistical complexity in the infodynamic analysis of sprays can be seen as part of the broader evolutionary trend of natural systems toward higher degrees of organization. By measuring and monitoring the statistical complexity of the droplet size distributions, insights into the evolution and adaptation of spray systems occurring over space and time can be obtained. Specifically, it can help answer questions such as: *How does the droplet size distribution in a spray evolve toward higher complexity under different operating conditions and nozzle designs?* This understanding aligns with the natural tendency of systems to move toward more organized complexity. Additionally, it can address the following: *What are the optimal conditions under which the spray achieves a balanced state of diversity and structure, ensuring both efficient atomization and desired droplet characteristics?* By framing these questions within the context of infodynamics, one can clarify the role of statistical complexity in driving the development of more sophisticated and effective spray systems, similar to the progression seen in natural systems.

Figure 5 structures the *complexity domain* map and characterizes each region. The limits of the complexity domain with no complexity are made of *fully regular* physical systems (*e.g.,* all droplets in the spray have the same size or the same velocity) and *fully chaotic* (e.g., all classes of drop sizes have the same sample size, resulting in a uniform distribution). A spray is often considered to be a complex flow, but its complexity has not yet been quantified. One of the goals of this study was to introduce an infodynamic perspective for measuring spray complexity.

In the following section, the Phase-Doppler Interferometer is considered an *infosensor*, which requires an explanation of this concept and its application to the measurement of more than one characteristic of the physical system. In the case of a spray, how can one know that the *infosensor* measured sufficient information on drop size and velocity?

3.2 Considerations on *infosensors*

A thermocouple is a sensor used to measure temperature through the electromotive force generated by the temperature difference between two junctions formed by two materials of different compositions measuring *informature* requires an *infosensor*, where the measurement principle is its ability to capture the statistical nature of a physical system. While the Seebeck effect explains how a thermocouple operates, the statistical analysis explains the operation of an *infosensor*. The two most relevant procedures in *infosensors*, as with any sensor, are their calibration and response times.

Calibrating an *infosensor* implies designing the best way to express the statistical nature of a physical system. For example, Panão (2022) showed that the decimal part of drop size measurements was redundant. Considering the microscale (μm) as the one that best describes drop sizes, it implies that building frequency probabilities of classes with less than 1 μm is pointless. Therefore, calibrating an *infosensor* involves identifying the scales of the elements in the phase space of the physical system and choosing an appropriate method to define the number of classes.

In the case of one measured characteristic of the physical system under infodynamic analysis, *informature* should be sufficient to assess the *infosensor* response time, as explored in Panão (2012). However, suppose that more than one characteristic is required to ensure that one acquires sufficient information (not data). In this case, mutual informature ($mH_{I,e}(d,u)$) should be used, which means that the amount of information contained in the drop size and velocity simultaneous measurements does not exceed the

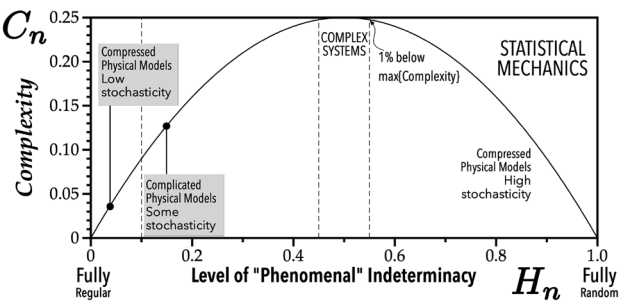

Fig. 5 Map of the dimensionless complexity domain

amount of information associated with each of these characteristics—$mH_{I,e}(d,u) \leq H_{I,e}(d) + H_{I,e}(u)$. This quantity depends on the joint probability between the measured quantities $p(d_i, u_j)$, which corresponds to the frequency probability associated with class d_i and class u_j such that $\sum_i \sum_j p(d_i, u_j) = 1$. The mutual informature corresponds to (Stone 2015)

$$mH_{I,b}(d,u) = \sum_{i=1}^{k_d} \sum_{j=1}^{k_u} p(d_i,u_j) \cdot \log_b \left(\frac{p(d_i,u_j)}{p(d_i) \cdot p(u_j)} \right) \quad (16)$$

where k_d, k_u are the number of size and velocity classes, respectively, b is the logarithm base (e.g., e leads to $mH_{I,e}$ measured in $nats$), $p(d_i) = \sum_{j=1}^{k_u} p(d_i,u_j)$ and $p(u_j) = \sum_{i=1}^{k_d} p(d_i,u_j)$. Figure 6 shows an example of response time calibration.

All the measured points resulted in response times lower than the maximum measurement time required to acquire $N = 5000$ samples of droplet characteristics. Figure 7 shows maps of the response time measurement and corresponding mutual informature.

The larger response time at the center and its lower mutual informature value indicate a region of high variability and independence between the sizes and velocities of the corresponding droplets. From the center of the spray to its outskirts, the amount of information of the size reduces the amount of information needed for the velocity, which is the meaning of higher mutual informature. Relative to the data acquisition time (Δt), the PDI mutual informature response times (τ, instant where $\left|1 - mH_{I,e}(t=\tau)/mH_{I,e}(max\{t\}\right| = 0.1$) had two clusters. Figure 8 shows the first cluster from locations at the outskirts of the spray that required less than 25% of the total acquisition time to stabilize mutual informature. By contrast, locations inside the spray require almost all samples to be acquired to ensure that the data contain sufficient information. These results for the PDI's informational response time are coherent with the lower data rates where the spray density is higher, requiring more time to stabilize the amount of local size-velocity mutual informature in the spray.

After this introduction and the presentation of the experimental setup, laser diagnostic technique, and the background concepts of an infodynamic analysis adapted to engineering, the results, and its discussion are addressed. Firstly, visualization and analysis concerning the breakup length are discussed, followed by an investigation of the droplet diameter released by the fragmentation of the ligaments and rim. Subsequently, the PDI technique results are presented in order to compare spray dynamics of conventional and alternative fuels for several AFRs. Afterward, the results focus on the mathematical nature of drop size distributions of conventional and alternative aviation fuel using infodynamics and present an attempt to measure the spray complexity and infodynamic properties.

4 Results and discussion

4.1 Visualization

The initial results and discussion concern visualization for a wide range of operating conditions using a high-speed camera to capture breakup structures in detail. The purpose is to provide insights into the breakup of conventional and alternative fuels, which will be further evaluated in terms of the mean breakup length. The visualization offers a qualitative analysis near the atomizer nozzle to enhance the understanding of the air–fuel interactions. Firstly, a sequence of images of HVO related to the 3^{rd} condition using an air flowrate of $\dot{m}_a = 0.11$ g/s is shown in Fig. 9. A continuous cylindrical body is detected from the nozzle. This liquid jet was subjected to airflow and began to destabilize while the liquid jet remained attached to the nozzle and elongated, its thickness gradually reduces. From Fig. 9a–c, the elongation of the liquid jet is noticeable with a large head droplet attached to its tip. As the liquid jet continued to extend and its thickness decreased, it became increasingly susceptible

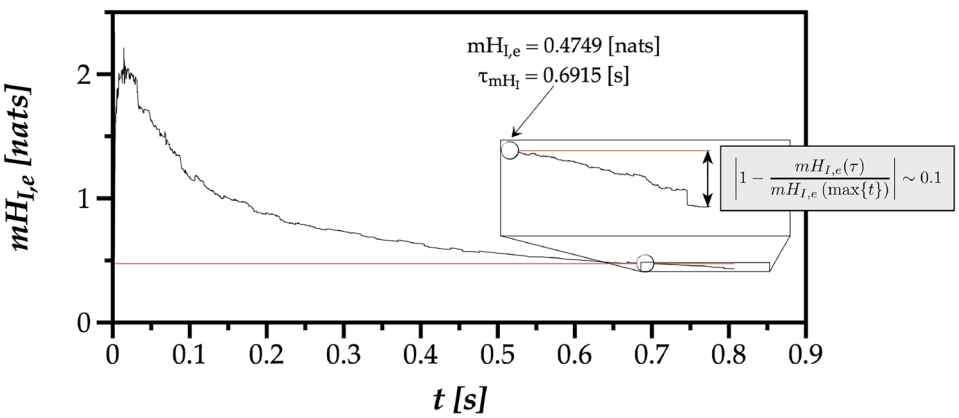

Fig. 6 Example of obtaining the response time for one measurement point

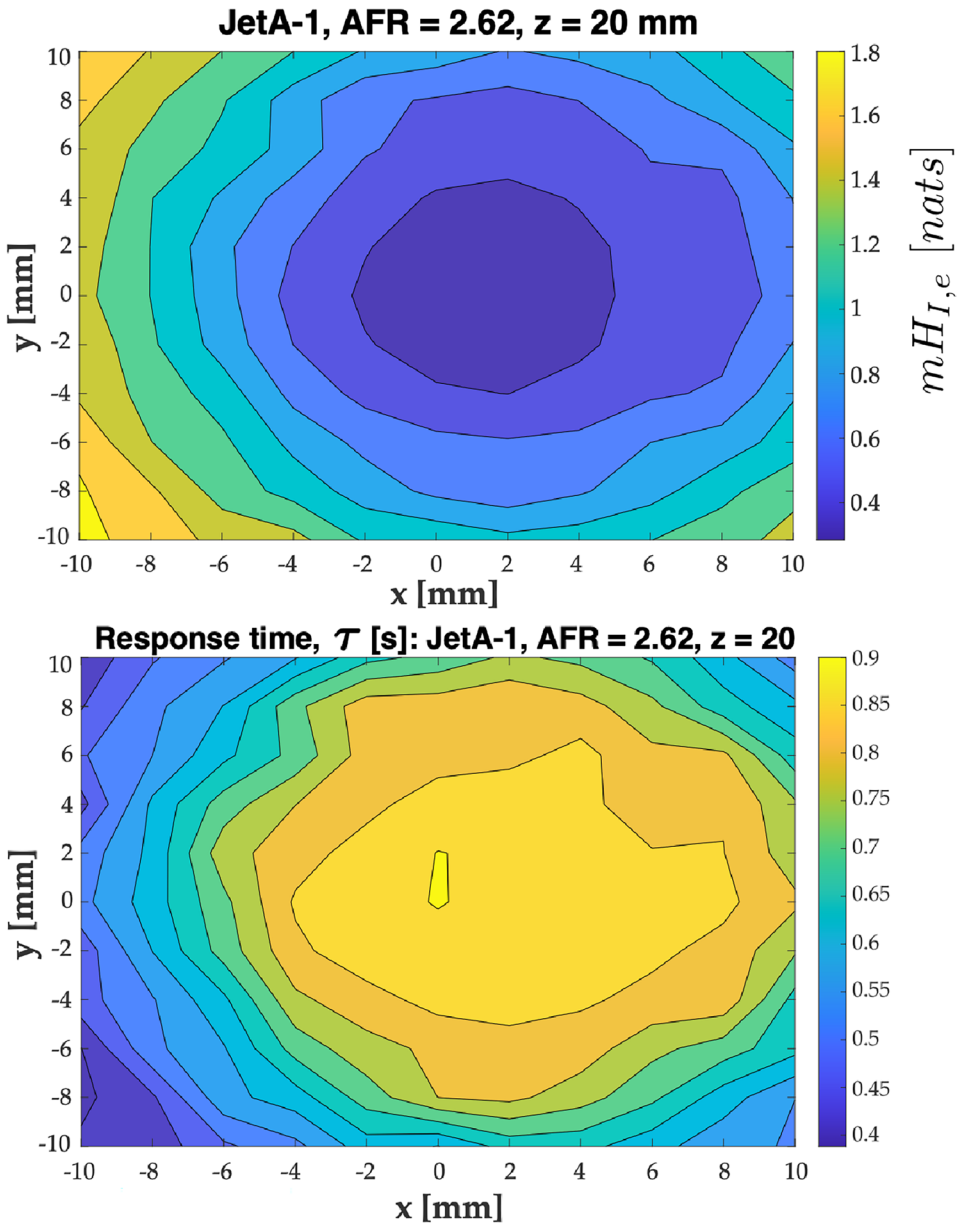

Fig. 7 Example of the mutual informature ($mH_{I,e}$ [*nats*]) map and corresponding the response time for HVO with an AFR = 2.62 at the $Z = 20$ mm measurement plane

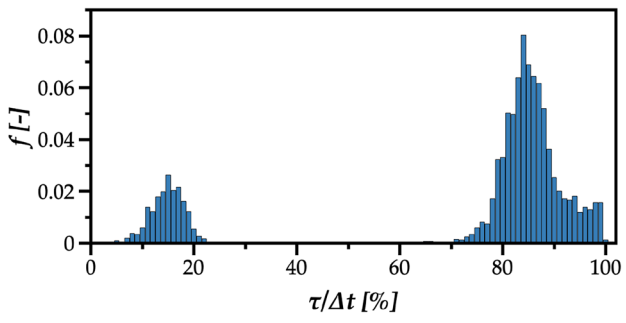

Fig. 8 Histogram of percentual response times in all measurement locations relative to the total measurement time taken to acquire 5000 samples

to disruption, as shown in Fig. 9e. Eventually, the ligament detached (Fig. 9e) from the nozzle breaks into small droplets downstream (Fig. 9f). Breakup occurs as a consequence of aerodynamic forces caused by the airflow in the liquid jet with a relatively low velocity, which increases the kinetic energy of the liquid phase and induces liquid stretching. Consequently, the liquid breaks when the aerodynamic forces overcome the surface tension.

To visualize the influence of the airflow on the HVO fuel, the air flowrate was doubled and the results are shown in Fig. 10. For this observation, the fuel flowrate was kept constant (3^{rd} condition in Table 4). A higher airflow reduces the liquid jet length, and compared to the jet shown in Fig. 9, there is no elongation of the thick liquid

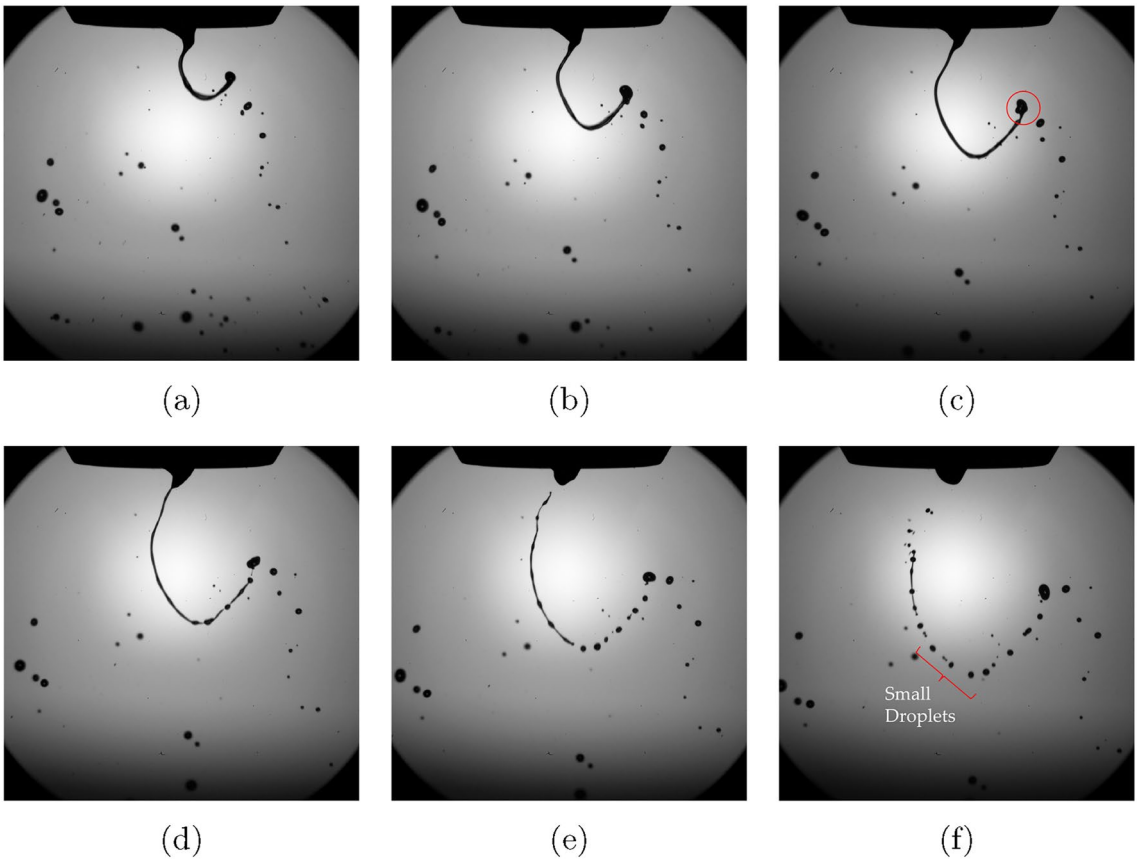

Fig. 9 Sequence of images of HVO equally spaced 0.75 ms under the following conditions: 3^{rd} fuel condition, $M = 2.5$, AFR = 1.73

portion. Instead, Fig. 10 shows bag formation and a thin balloon- or bag-like structure near the nozzle (Fig. 10b). In this case, the breakup of the liquid portion is initiated as a consequence of bag formation, which eventually disrupts and produces extremely small droplets. For this particular condition, measurements of the droplet diameter were not feasible for these setup conditions.

Figures 11 and 12 show the sequence of images for HVO and Jet A-1, respectively. For this visualization, the fuel flowrate was maintained constant, similar to the previous conditions (5th condition), and the air flowrate ($\dot{m}_a$) was 0.11 g/s. A bag breakup is spotted in both Figs. 11 and 12. Bag formation occurs promptly and near the atomizer nozzle for higher airflow, highlighting the influence of increasing the airflow. The bag breakup is more catastrophic, leading to a more effective disruption of the rim and allowing the detection of considerably smaller droplets. In addition, the frequency of this phenomenon was higher when the airflow was increased.

4.2 Breakup length analysis

A more detailed examination of the breakup length is required for an alternative jet fuel comparison in order to better understand the air–liquid interaction. In this respect, the visualization provides information regarding the breakup characteristics, allowing measurements of its length. The analysis of the primary atomization region is typically characterized by the jet breakup length, which is a signature of the atomization quality, as previously stated by Kumar and Sahu (2018) and the source indeterminacy in spray information. Figure 13 shows the mean breakup length normalized by the liquid bore diameter for HVO and Jet A-1, respectively. The error bars in Fig. 13 correspond to the standard deviation of the mean breakup length normalized by the liquid diameter orifice. Breakup analysis is a function of the momentum flux ratio and is a relevant parameter for evaluating the length of an unbroken liquid core (Lasheras 2000). According to (Lasheras 2000; Reitz and

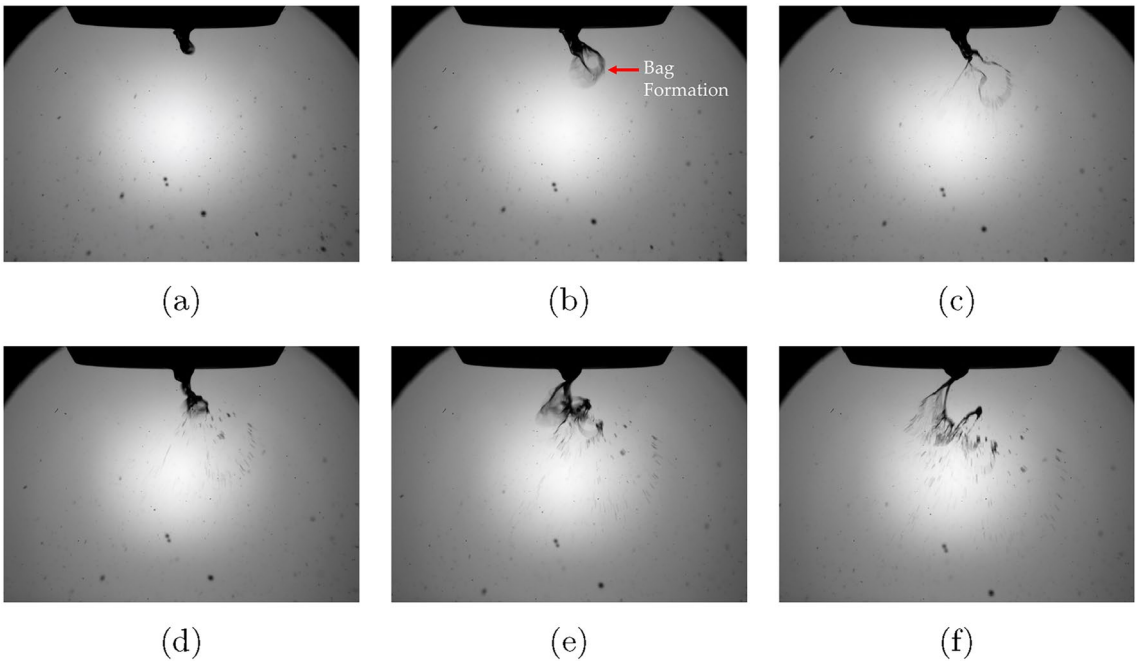

Fig. 10 Sequence of images of HVO equally spaced 0.25 ms under the following conditions: 5th fuel condition, $M = 9.98$, AFR = 3.45

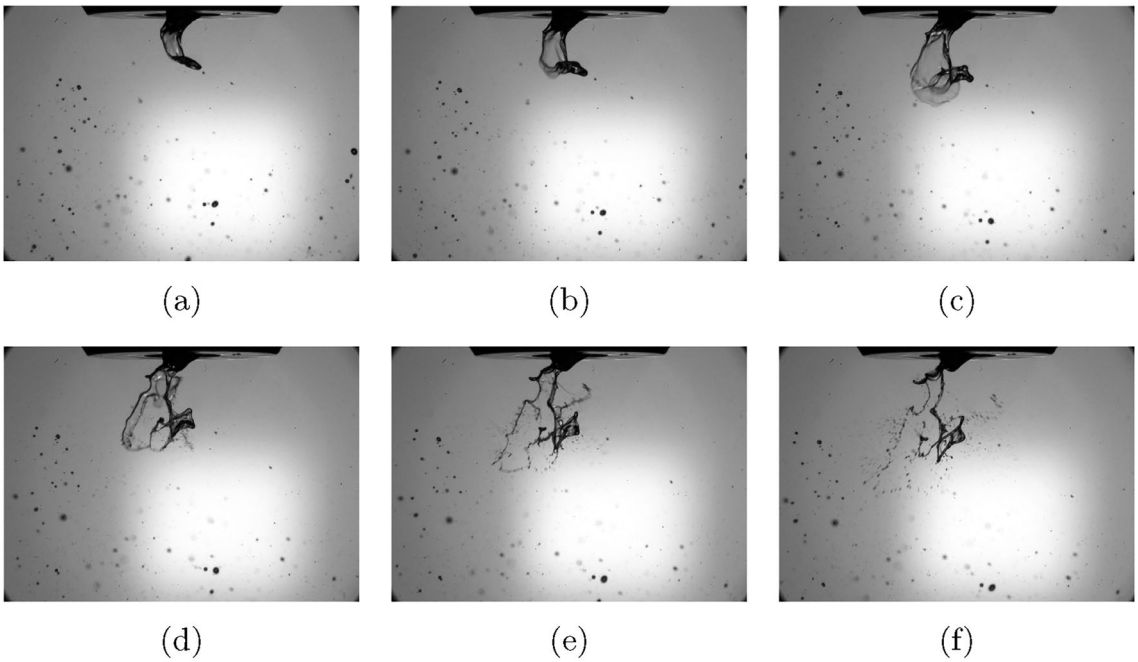

Fig. 11 Sequence of images of HVO equally spaced 0.185 ms under the following conditions: 5th fuel condition, $M = 2.94$, AFR = 1.87

Bracco 1982), if M ≪ 1, the breakup is governed by the liquid jet. However, if M≥ 1, the breakup length is determined by the gas jet, whereas for considerably high M values, the length is very short. The breakup length corresponded to the maximum length in the axial direction from the nozzle liquid jet rupture point. The expressions presented in Fig. 13 were developed based on the experimental data of the fuels and the Leroux et al. (2007) correlation. Given the significance of the momentum flux ratio and the specific operating conditions of this study, the application of the Leroux et al.

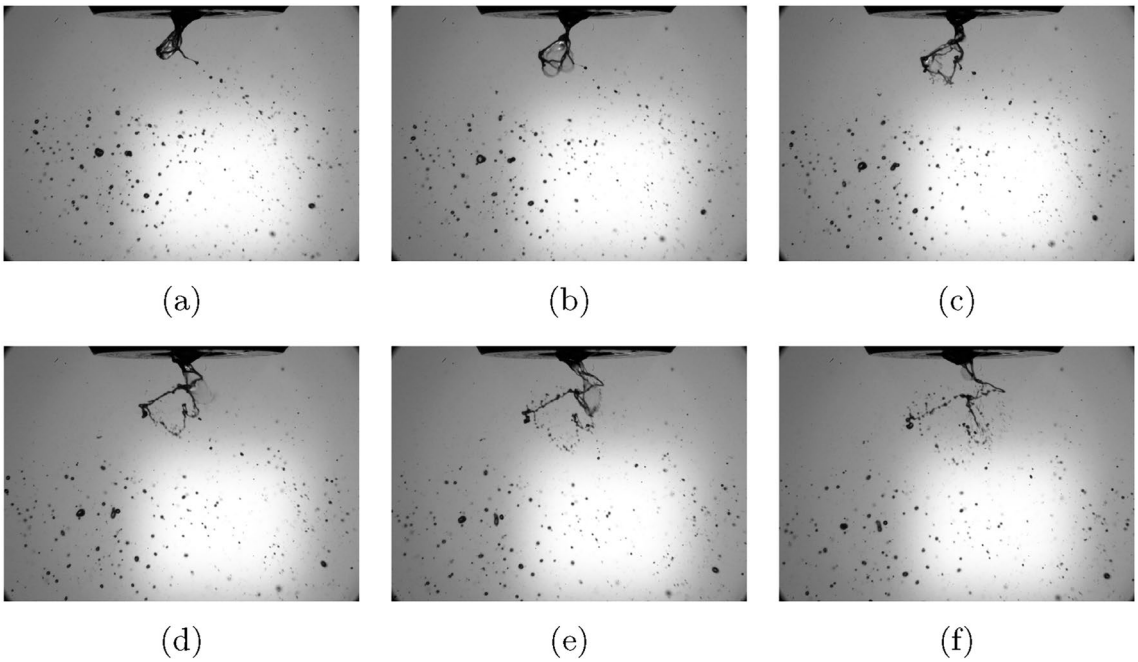

Fig. 12 Sequence of images of Jet A-1 equally spaced 0.185 ms under the following conditions: 5th fuel condition, $M = 4.0$, AFR = 2.21

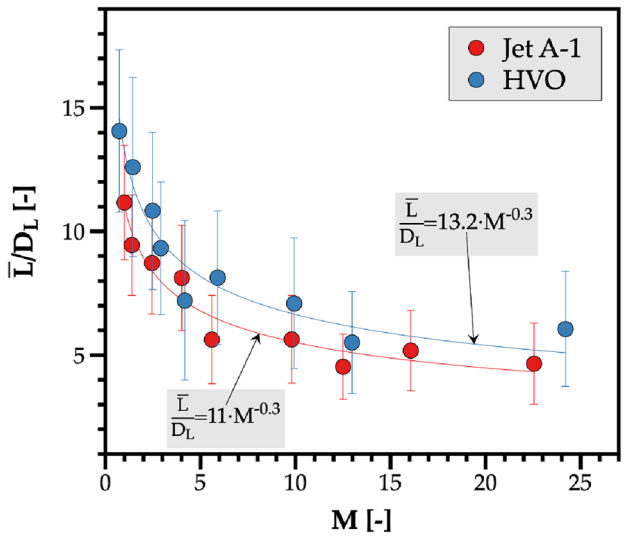

Fig. 13 Normalized mean breakup length as a function of momentum flux ratio (M) for HVO and Jet A-1

(2007) expression was deemed the most appropriate choice for evaluating the normalized breakup length, as will be further discussed. In particular, the power of the normalized correlation is equal for Jet A-1 and HVO. This analysis was developed based on experimental data regarding breakup length and the Leroux et al. (2007) correlation. The power of the normalized correlation corresponds to the decay rate effect of M over L/D, which aligns with the Leroux et al. (2007) formulation. Additionally, a slight adjustment to the parameter scale resulted in a better fit to the experimental data, prompting us to consider the potential influence of an additional effect related to viscosity, as will be discussed later. The similarity in the power of the normalized correlation may arise from the influence of inertia (similar density values) and surface tension forces on primary atomization, overshadowing viscous forces. Additionally, it should be emphasized that the operating conditions of this study closely align with those of Leroux et al. (2007), further supporting the applicability of their correlation, which may also clarify the observed similarity. The equality of the exponent for Jet A-1 and HVO suggests potential universality. However, to confirm this observation, further analysis using fuels with distinct physical properties is necessary.

Analyzing Fig. 13, the results show that increasing the momentum flux ratio reduces the normalized mean breakup length, regardless of the fuel used. For considerably lower M values, the normalized mean breakup length decreases sharply. As the momentum flux increases, it converges at a constant rate. Additionally, the breakup length of HVO is slightly higher than that of Jet A-1, which may be attributed to the higher viscosity of the biofuel, as shown in Table 3. Comparing the results with the operating conditions provided in Table 4, it can be observed that an increase in the air flowrate leads to a shorter breakup length, and the opposite tendency is observed for the increase in the fuel flowrate. This effect was pronounced by the aerodynamic force on liquid disintegration. A higher airflow is related to a higher

We_a, which can be explained by the increased shear stress acting on the fuel–air interface. Similar findings have been reported by (Roudini and Wozniak 2018; Kumar and Sahu 2018).

Several correlations have been reported in the literature to predict the mean breakup length, as listed in Table 2. Consequently, from the experimental results obtained in the present study, an empirical equation was formulated to predict the mean breakup length produced by an air-assisted atomizer with a swirl. Figure 14 shows the empirical correlation obtained in this study, highlighted by the blue dashed line using the normalized mean breakup length results for HVO and Jet A-1.

If the correlation follows the format of Leroux et al. (2007), it would be equal to $\frac{\bar{L}}{D_L} = 12M^{-0.3}$ with $R^2 = 0.9282$, as shown in Fig. 14 which includes correlations found in the literature. The maximum and minimum standard deviations for the normalized mean breakup length were 3.42 and 1.30, respectively. This correlation indicates that the normalized mean breakup length exhibits a power law relationship with the momentum flux ratio, in accordance with the previous correlations (Leroux et al. 2007; Zhao et al. 2014; Kumar and Sahu 2018). The correlation proposed by Kumar and Sahu seems to underpredict the experimental data, a discrepancy that may be attributed to the influence of an optical connectivity technique. Moreover, Leroux et al. (2007) considered the lower limit of $\mathrm{Re}_L = 45$, and the Reynolds numbers for the HVO were below the limit, which could imply a higher effect of viscosity relative to inertia, leading to longer breakup lengths and justifying an increase in the scale parameter from 10 to 12. Therefore, following the relevance of the Reynolds number, an alternative empirical correlation results in

$$\frac{\bar{L}}{D_L} = 23.7M^{-1/3}\,\mathrm{Re}_L^{-1/5}, \tag{17}$$

with a correlation coefficient between experimental and predicted data of $R^2 = 0.9642$. The operating conditions for the correlation are defined by $19.1 \le Re_L \le 144.4$, $1.4 \le \mathrm{We} \le 60.1$ and $0.7 \le \mathrm{M} \le 54.4$.

As noted previously, higher values of M have progressively smaller effects on the normalized mean breakup length. To evaluate this observation, the concept of diminishing returns is introduced. Figure 15 shows the diminishing returns concerning the normalized mean breakup length as a function of the momentum flux ratio for HVO and Jet A-1. This purpose is accomplished by the derivative of normalized breakup length with respect to the momentum flux ratio being equal to 0.1 to identify from which the returns are diminished, represented by a horizontal dashed line shown in Fig. 15. Beyond this line, decreasing the normalized mean breakup length implies an increase in M by more than an order of magnitude. For Jet A-1, the diminishing return line intersects at $M = 14.7$, whereas for HVO, it occurs at $M = 17$.

Figure 16 shows the analysis of the breakup length concerning the discrete differential informature as a function of the momentum flux ratio for HVO and Jet A-1. The purpose is to obtain an information perspective to gain a deeper understanding of the primary atomization challenge. The result shows that Jet A-1 possesses relatively lower $H_{\Delta,e}$ values. Regardless of the fuel employed, the $H_{\Delta,e}$ declines as M increases. However, a transition in the $H_{\Delta,e}$ pattern is detected at $\mathrm{M} \approx 14$, indicating a regime transition nearly

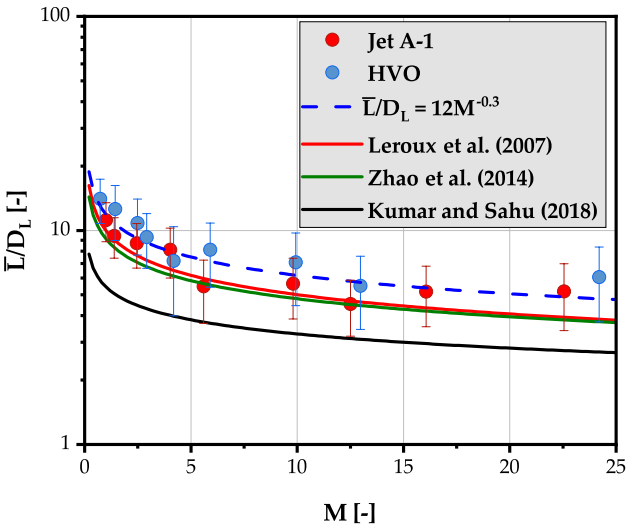

Fig. 14 Normalized mean breakup length correlations

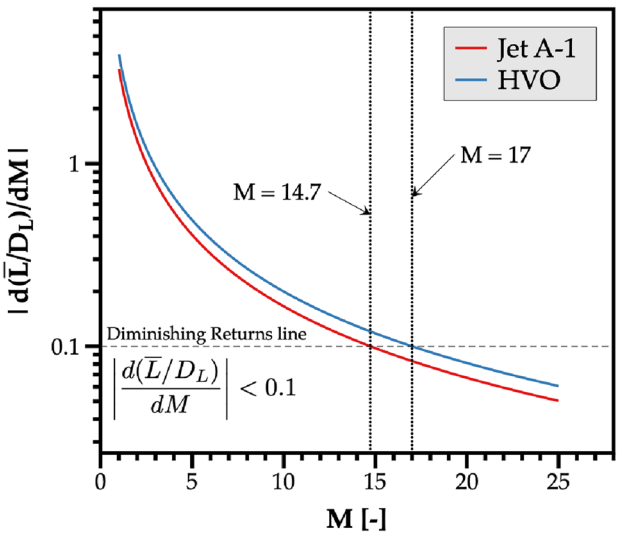

Fig. 15 Diminishing returns concerning the normalized mean breakup length as a function of the momentum flux ratio for HVO and Jet A-1

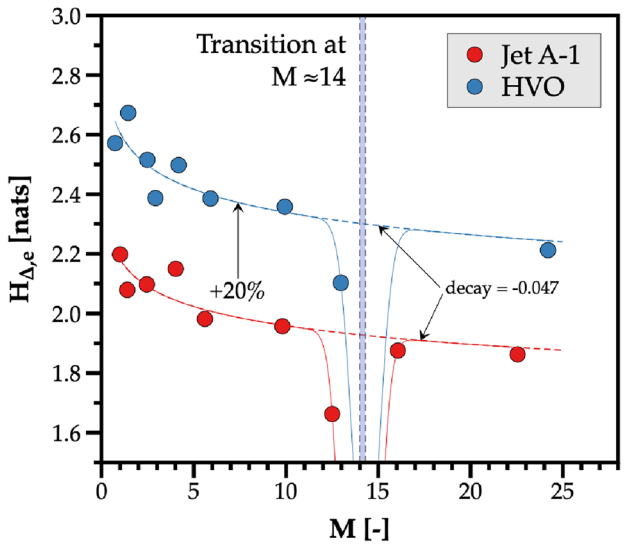

Fig. 16 Discrete differential informature as a function of the momentum flux ratio for HVO and Jet A-1

similar for both fuels. This transition was determined by subtracting the decay function ($H_{\Delta,e}$) from a function that determines M_t:

$$H_{\Delta,e} = aM^{-b} - C\exp\left(-\left(M - M_t\right)^2\right) \tag{18}$$

where a, b, C depend on the fuels considered. This observation highlights that for M values higher than 14, the atomization is finer, given the relevance and dominance of air in the atomization process. To complement the conventional breakup length analysis, discrete differential informature analysis was conducted, offering an informational perspective that fosters a deeper understanding of the primary atomization challenge. Thus, a transition in the $H_{\Delta,e}$ pattern is detected at M ≈ 14, indicating a regime transition that is nearly identical for both fuels, with a slight decrease in the transition value. The present study confirms that the atomization process transitions from hydrodynamic-dominant atomization to aerodynamic atomization between M = 14 and M = 17. The combination of image data processing and infodynamic analysis provides a robust approach to comprehensively characterize spray behavior. Additionally, this analysis concerning infodynamics agrees with the literature underlying that for M higher than 10 (Hopfinger and Lasheras 1994) or, more specifically, 13.3 (Dunand et al. 2005) leads to finer and better atomization.

4.3 Droplet diameter analysis

An investigation dedicated to the droplet diameter released after the primary atomization was performed for the highest fuel flowrate. This analysis is a qualitative approach since the procedure implemented discards repeated droplets with identical diameters. Consequently, this result will provide information regarding the range of diameters released by the fragmentation of the ligaments and rims. Repeated droplets are not considered in the analysis, and a tracking method should be employed in future studies. Droplets with an eccentricity equal to or higher than 0.6 are considered for analysis. Regarding the operating condition, only the highest fuel flowrates were explored. Thus, the 5th condition presented in Table 4 under two airflows is investigated. These working conditions were selected due to the reduced diameter of the droplets with lower fuel flowrates which can be challenging to predict its diameter with accuracy. Figure 17 shows the diameter of the droplets released by the fragmentation of the ligaments and rims for HVO and Jet A-1.

For the purpose of this analysis, the 5th condition was examined, and histograms using variable bin widths were analyzed due to multimodal droplet size distribution (Panão 2022). Additionally, Gamma and Log-normal mathematical probability functions were considered to understand the organization of droplet size data. Regardless of the fuel employed, increasing the air flowrates leads to a reduced droplet diameter. For the lowest airflow ($\dot{m}_a$ = 0.11 g/s), larger droplets are released, possessing mainly diameters ranging from 0.5 to 1.0 mm. This finding can be related to the mean breakup length. Following the previous results, higher $\dot{m}_a$ leads to a shorter breakup length, resulting in secondary droplets with smaller diameters. Thus, the atomization efficiency is proven to be related to the jet breakup length. An in-depth understanding of the jet breakup is essential to understanding the droplet size and the spatiotemporal distribution of the liquid mass in the vicinity of the reaction zone downstream of the atomizer nozzle (Kumar and Sahu 2018). Regarding the probability mathematical functions, results for Log-Normal and Gamma are presented in Fig. 17a–d, respectively. This analysis aims to investigate which probability mathematical functions can describe the experimental droplet data. For the lowest airflow ($\dot{m}_a$ = 0.11 g/s), Gamma produces an overall better fitting, as displayed in Fig. 17c. Consequently, it is noticed that for the ligament breakup, the droplet size distribution can be represented by a Gamma distribution. This observation was already reported by Panão et al. (2020); Villermaux et al. (2004). Similar observations were achieved by increasing the airflow. However, it is important to highlight that only the droplets released by the rim fragments are analyzed in the present work. The disruption of the bag produces considerably small droplets, which cannot be investigated due to the limitations of the current experimental setup.

Figure 18 shows a fuel comparison in terms of secondary droplet diameter using a Gamma distribution. The background reason for using the Gamma distribution is rooted in the work of Villermaux et al. (2004), who associated the

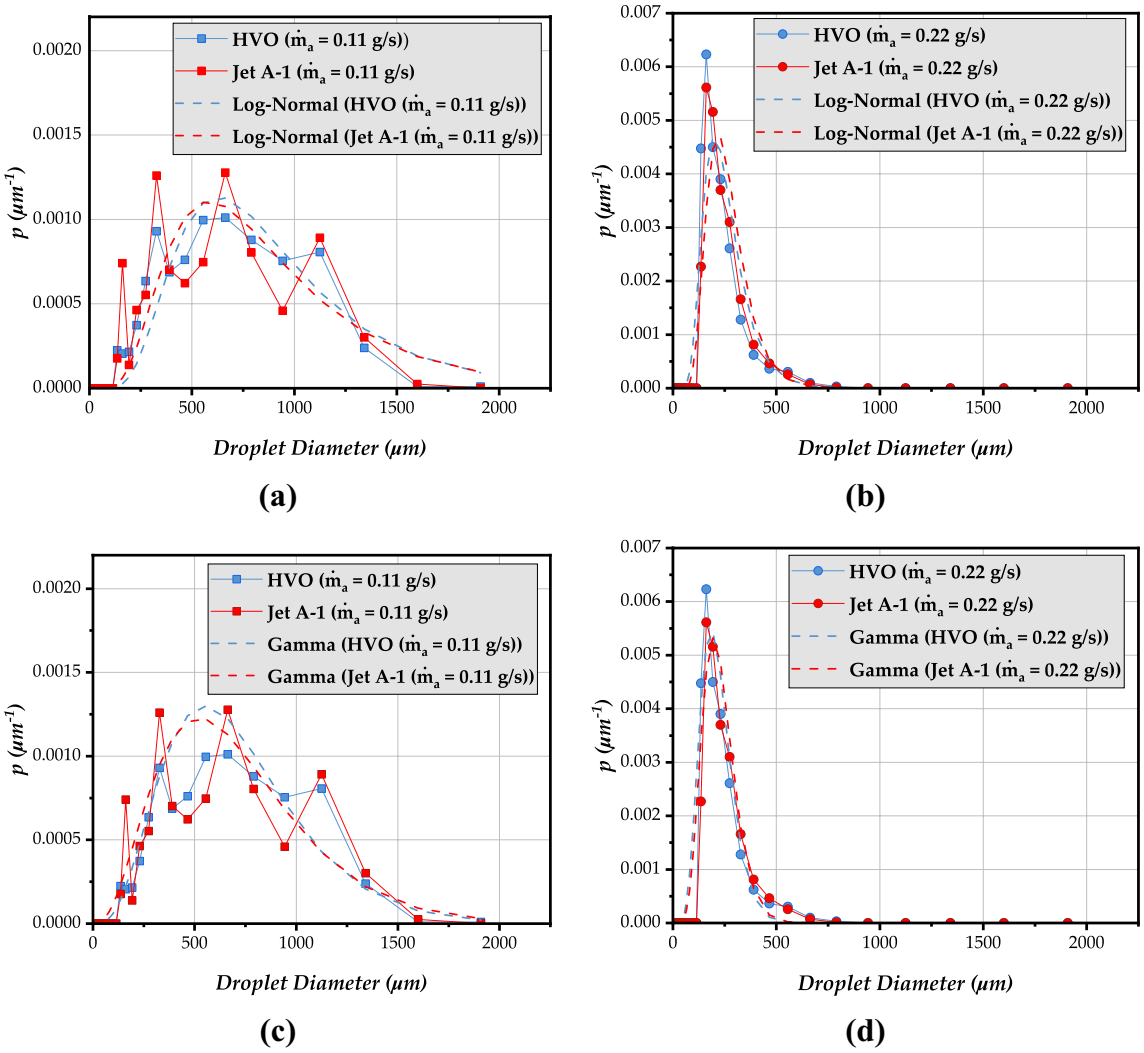

Fig. 17 Probability density distribution of droplet diameter considering the 5th condition under two air flowrates **a**, **b** with a Log-Normal and **c**, **d** Gamma distribution

Gamma distribution function with the outcome of ligament temporal fragmentation, modeling each ligament as an aggregation of sub-droplets arranged in several sub-layers. For this examination, the 5th condition was investigated for two air flowrates. A higher $\dot{m}_a$ leads to shorter secondary droplets regardless of the fuel employed. Concerning the fuel comparison, a marginal difference in the droplet diameter is observed. Moreover, additional operating conditions should be explored in order to understand if the tendency is maintained.

4.4 Phase Doppler interferometer results

The current subsection is dedicated to the experimental results and discussion of phase Doppler interferometry (PDI) for conventional and alternative jet fuels. The PDI technique was employed to acquire quantitative measurements of the droplet size and velocity in the radial and axial directions to better understand spray dynamics. The present discussion serves as a pivotal investigation for further analysis of the infodynamic nature of the liquid atomization of Jet A-1 and HVO. Concerning the droplet size distribution, the Sauter mean diameter (D_{32}) was evaluated to avoid potential misinterpretations associated with the arithmetic mean. In this context, D_{32} is an indicator of the atomization efficiency (Panão 2022) suitable for heat and mass transfer applications, given by the ratio of the total droplet volume to their surface areas, as presented in the following expression:

$$D_{32} = \frac{\sum_{i=1}^{n} n_i d_i^3}{\sum_{i=1}^{n} n_i d_i^2} \tag{19}$$

Figure 19 shows the influence of the spray development characteristics on the axial velocity and the Sauter mean

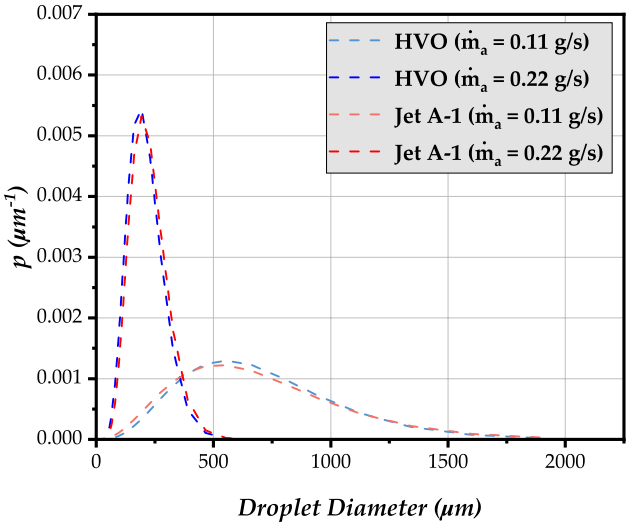

Fig. 18 Fuels comparison of droplet diameter distribution considering the 5th condition under two air flowrates using Gamma distribution

diameter for HVO considering an AFR ≈ 8, respectively. Four axial distances were considered: Z = 5, 10, 15, and 20 mm. The results show that by increasing the distance from the nozzle, the interaction with the surrounding environment reduces the axial velocity, and the SMD decreases. However, the SMD profile seems to stabilize for Z ≥ 15 mm, indicating that the spray is fully developed. The differences observed until Z = 15 mm suggest that atomization occurs simultaneously with the dispersion of the generated droplets, and it is difficult to distinguish the relative contribution of each mechanism to spray formation and growth.

Additionally, the highest values for the axial velocity are present in the central region of the spray. In the alignment, the lowest SMD values were also found in the core area. Larger droplets with reduced axial velocity were observed in the boundary region because the swirling flow was centrifuged outward. This observation indicates that as the radial distance increases, the axial velocity decays, and the highest value for the axial velocity is closer to the centerline of the atomizer. However, the results indicate that the spray is not symmetrical, which may be attributed to the presence of the swirl, as previously mentioned. Following the analysis of the influence on the spray characteristics of the axial and radial distances, the impact of the air–fuel ratio variations was addressed. The purpose is to understand how the AFR affects the spray dynamics.

Figure 20 shows the influence of the fuel and air mass flow on the axial velocity and the Sauter mean diameter for HVO at an axial distance of Z = 15 mm. Three air–fuel ratio (AFR) conditions were examined in this study: (1) maintaining a constant air mass flowrate while increasing the fuel mass flowrate and (2) increasing the air mass flowrate while keeping the fuel mass flowrate constant. The results show that the fuel mass flowrate affects the Sauter mean diameter but not the spray velocity, while the air mass flowrate affects the size and velocity of the droplets in the spray. These results are relevant from the perspective of controlling the spray characteristics. Namely, the fuel mass flowrate affects the size scale but not the SMD profile. This means that the fuel mass flowrate does not change the atomization

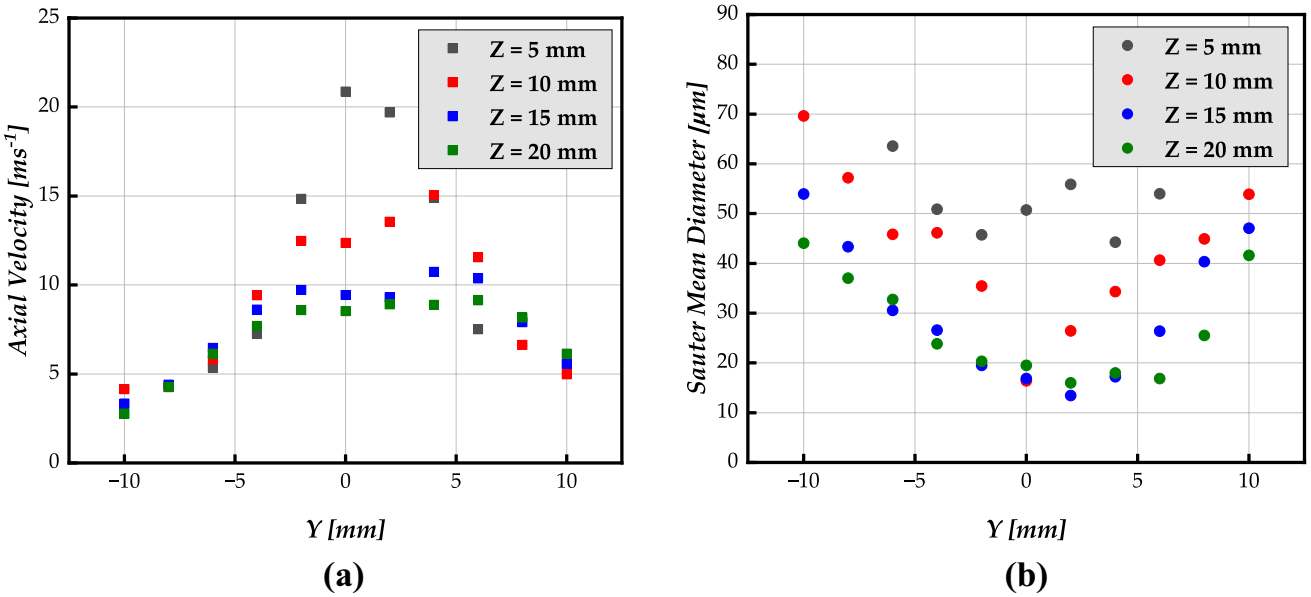

Fig. 19 Influence of the axial distance for HVO considering an AFR ≈ 8: **a** Axial velocity; **b** Sauter mean diameter

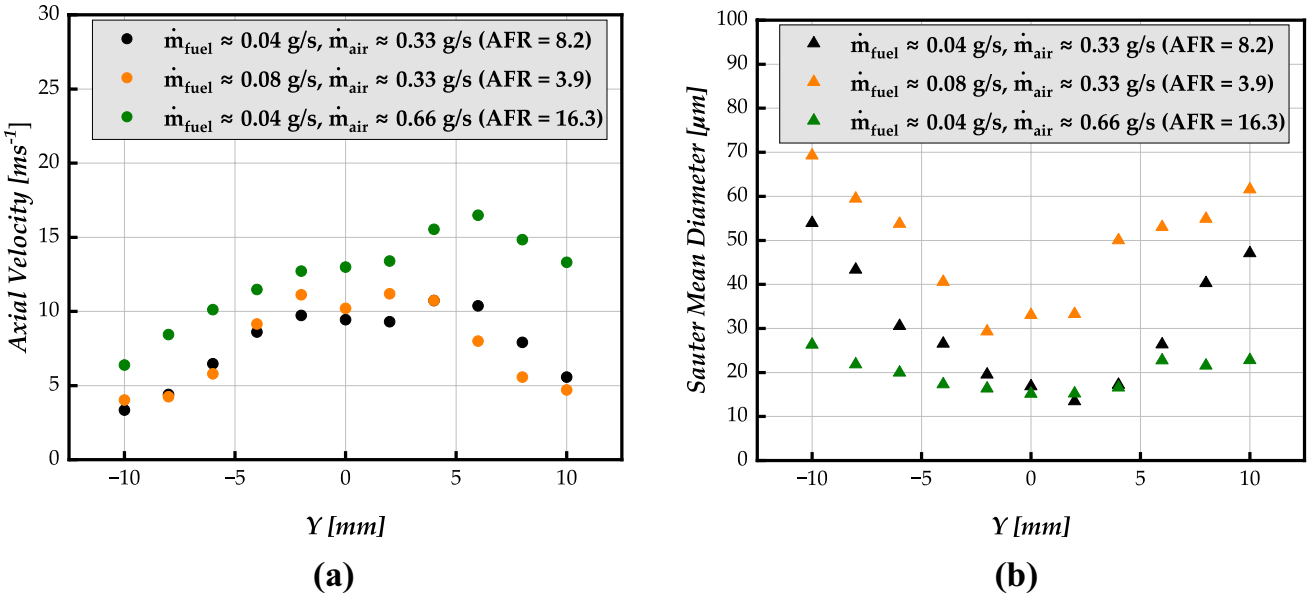

Fig. 20 Influence of the fuel and air mass flowrate for HVO at $Z = 15$ mm: **a** axial velocity; **b** Sauter mean diameter

mechanism. On the contrary, the air mass flowrate changes both the size and velocity, modifying the spray morphology and affecting the atomization mechanism. As the AFR increases, the energy available to break down the fuel jet into smaller droplets increases, resulting in a more effective disintegration of the fuel jet into smaller droplets.

Other works corroborate that the increase in the relative velocity promotes a more significant instability in the liquid (Kumar et al. 2021; Rizkalla and Lefebvre 1975). For a lower AFR, the kinetic energy of the atomizing air is insufficient to overcome the viscous and surface tension forces hindering liquid atomization, which is evident in the boundary region owing to the reduced effect of the aerodynamic shear forces. This would explain why the spray pattern exhibited a more uniform Sauter mean diameter for a constant fuel flowrate and a higher air velocity, leading to a high AFR. Concerning the effect of the fuel mass flowrate Beck et al. (1991) reported that a decrease in AFR induced by a higher liquid mass flowrate, indicates that the amount of air momentum per unit mass of liquid reduced, becoming insufficient for integrating the liquid phase to the same degree. In practice, their work supports the dominant effect of the aerodynamic forces over liquid atomization after the primary breakup stage. Still, the present results add that more fuel means droplets with more mass (larger SMD) without affecting the mechanism.

After discussing the overall spray dynamics and the influence of the AFR variation on HVO, a comparative analysis of conventional and alternative jet fuels concerning SMD is presented in Fig. 21. The purpose was to better understand the impact of the AFRs on the differences produced concerning the droplet size distribution radial profile at Z = 15 mm. To ease the interpretation, the data points are connected by colored lines where the red color corresponds to Jet A-1, while the blue is referent to HVO. Figure 21a shows that Jet A-1 possesses a slightly lower Sauter mean diameter, which can be related to the high viscosity of HVO compared with Jet A-1. However, as the air flowrate increased to approximately 0.55 g/s, the Sauter mean diameter for HVO and Jet A-1 showed nearly identical values. This observation highlights the significant influence of aerodynamic forces on the overall dynamics of spray formation. Previous studies have highlighted that in twin-fluid atomizers, more specifically airblast atomizers, the liquid velocities are relatively smaller than those of the pressure nozzle. Consequently, the droplet diameter tends to be less sensitive to variations in liquid viscosity (Lefebvre and McDonell 2017), explaining the marginal differences measured between fuels. The droplet size of liquids with low viscosity, such as water and kerosene, is mainly governed by liquid surface tension, air density, and velocity.

However, in liquids with high viscosity, the effects of air properties are less predominant, and SMD becomes more dependent on the liquid properties (Lefebvre 1980). In light of this, for liquids of low viscosity, the mean droplet size is inversely proportional to the relative velocity between the air and the liquid, whereas for large values of AFR, the influence of viscosity on SMD becomes negligibly small (Lefebvre and McDonell 2017). As noted previously, high values of AFR correspond to larger air velocities that can promote prompt atomization, leading to a rapid and violent disruption of the liquid jet, where the effects of liquid

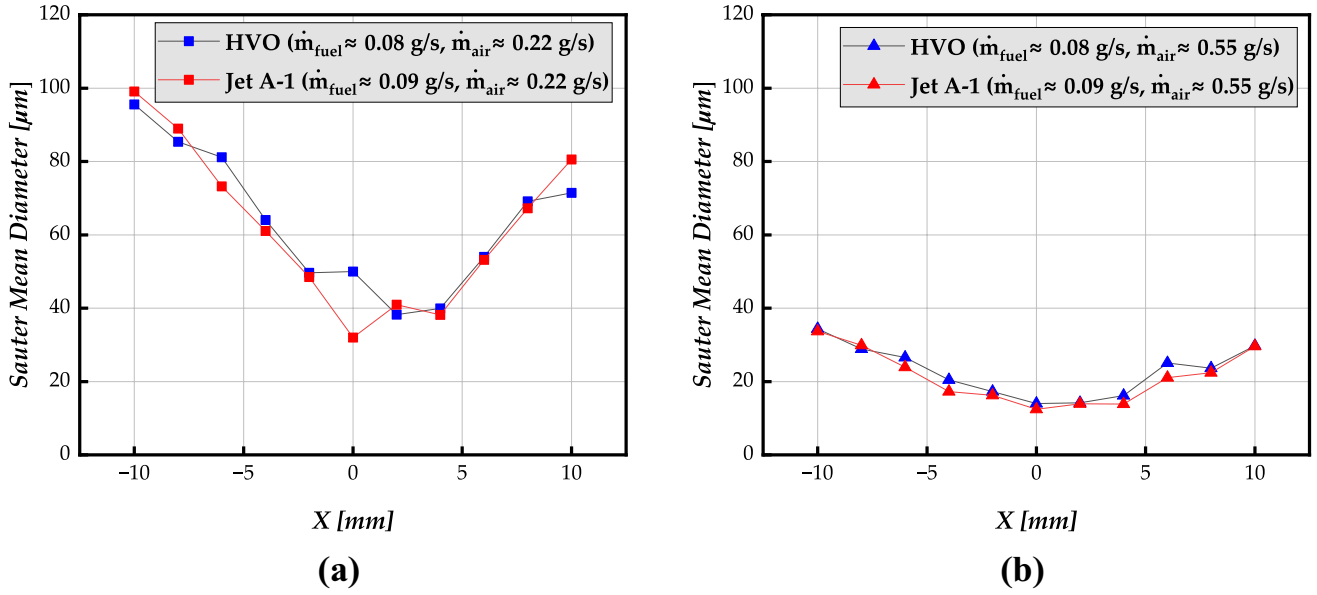

Fig. 21 HVO and Jet A-1 comparison in terms of SMD for a constant fuel flowrate and different air flows at $Z = 15$ mm: **a** $\dot{m}_{air} \approx 0.22$ g/s; **b** $\dot{m}_{air} \approx 0.55$ g/s

viscosity are minor ($U_a > 20$ m/s) (Urbán et al. 2017; Lefebvre 1992). Based on this, the experimental results provided in Fig. 21 are in agreement with the literature findings, indicating that increasing the AFR leads to an overall similar spray behavior between the fuels. In addition, the viscosity variation between HVO and Jet A-1 does not differ in the order of magnitude to produce a significant effect on the mean droplet size, as previously discussed. Overall, the findings suggest that Jet A-1 and HVO behave similarly during the atomization process. These results are significant in researching alternative energy sources for aviation, reinforcing the idea that sustainable and green fuels can be used to address environmental concerns. Therefore, regarding atomization analysis, HVO is a biofuel that produces sprays with similar characteristics to those produced by conventional aviation fuels.

The preceding analysis is dedicated to the planar distributions at Z = 15 mm for SMD and the axial velocity for HVO and Jet A-1, as shown in Figs. 22 and 23, respectively. The purpose was to extend the radial analysis previously done to a spatial perspective of the different AFRs.

Regardless of the fuel tested, an increase in the AFR reduces the SMD in both the X- and Y-axes, with the decrease being approximately equal in both directions. Despite the AFR being considered, the larger droplet diameters are presented mainly on the periphery of the spray, whereas the lower SMD is spotted in the central region, leading to a "bowl" shape. In addition, the increase in the AFR results in a spray with lower drop size diversity for both conventional and alternative jet fuels, as previously discussed. Regarding the axial velocity, the planar distribution indicates that the spray is not entirely symmetrical and is more evident at the highest AFR. This observation contrasts with the previously discussed SMD distribution. A possible explanation is that an increased air flowrate enhances the swirl effect, which becomes more perceptive but is independent of drop formation.

4.5 Infodynamic nature of liquid atomization

In the first part of this section, the informational results of the spray explore the infodynamic nature of liquid atomization, and whether discrete representations of drop sizes correspond to any of the common mathematical probability distribution functions associated with sprays. In the second part, an attempt is made to investigate informational properties based on infotropies as "contextualized" informatures to address the challenge of quantifying spray complexity.

The purpose of fitting probability mathematical functions to discrete drop size distributions is to understand the nature of liquid atomization processes. In the present Jet A-1 and HVO comparison, most properties were similar, except for the dynamic viscosity, as shown in Table 3. If this property affects the nature of liquid atomization using the same atomizer and liquid breakup strategy, different mathematical functions would fit the experimental data.

The three essential probability mathematical functions typically used to fit drop size distribution data are Log-normal, Gamma, and Weibull. The best and most well-known goodness-to-fit test is the Kolmogorov–Smirnov (KS) test, which compares two continuous distributions and is sensitive to the test sample size. Other methods compare two

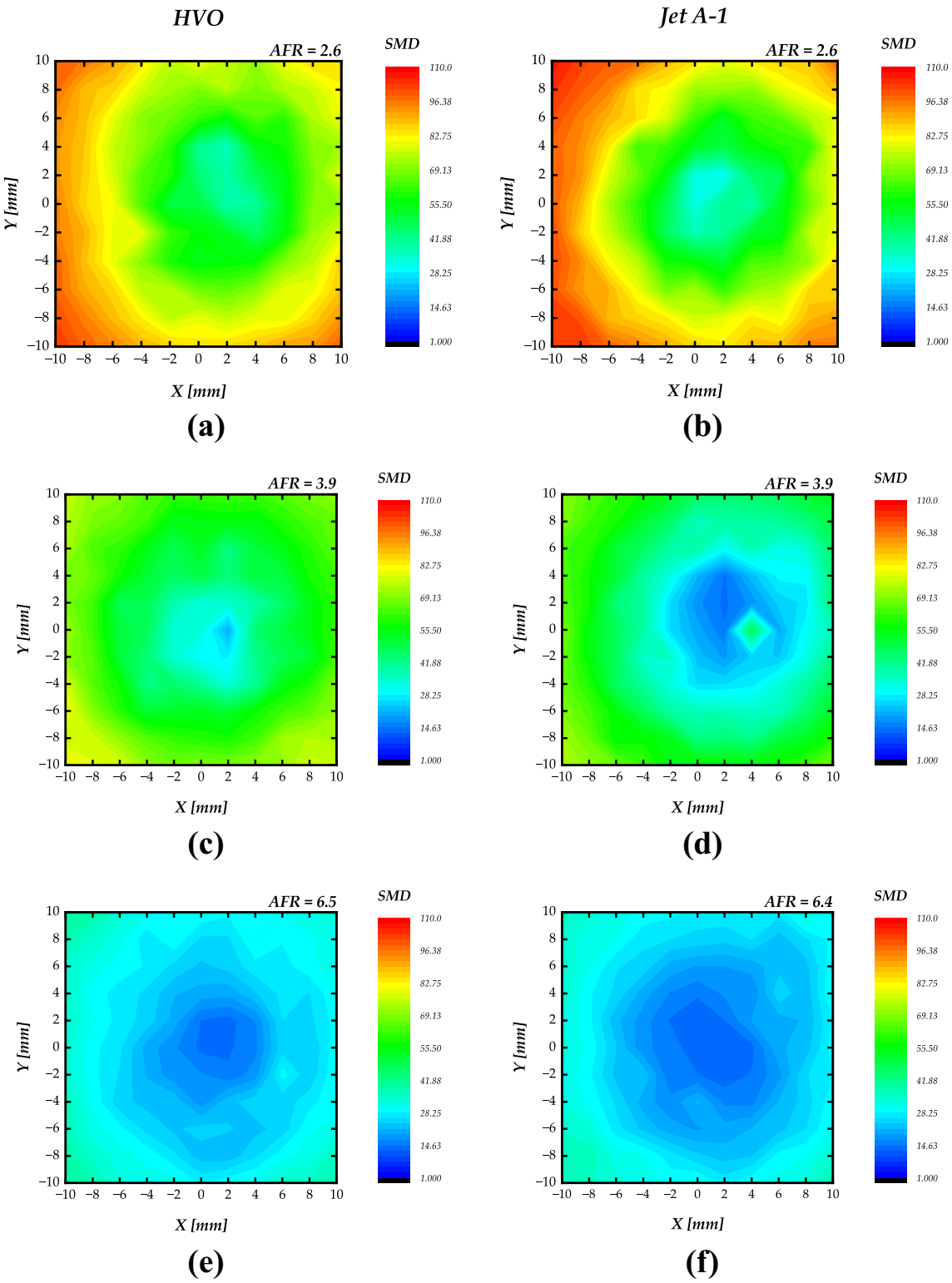

Fig. 22 Contour of the Sauter mean diameter (μm) for X and Y radial distances for HVO: **a** AFR = 2.6; **c** AFR = 3.9; **e** AFR = 6.5. For Jet A-1: **b** AFR = 2.6; **d** AFR = 3.9; **f** AFR = 6.4

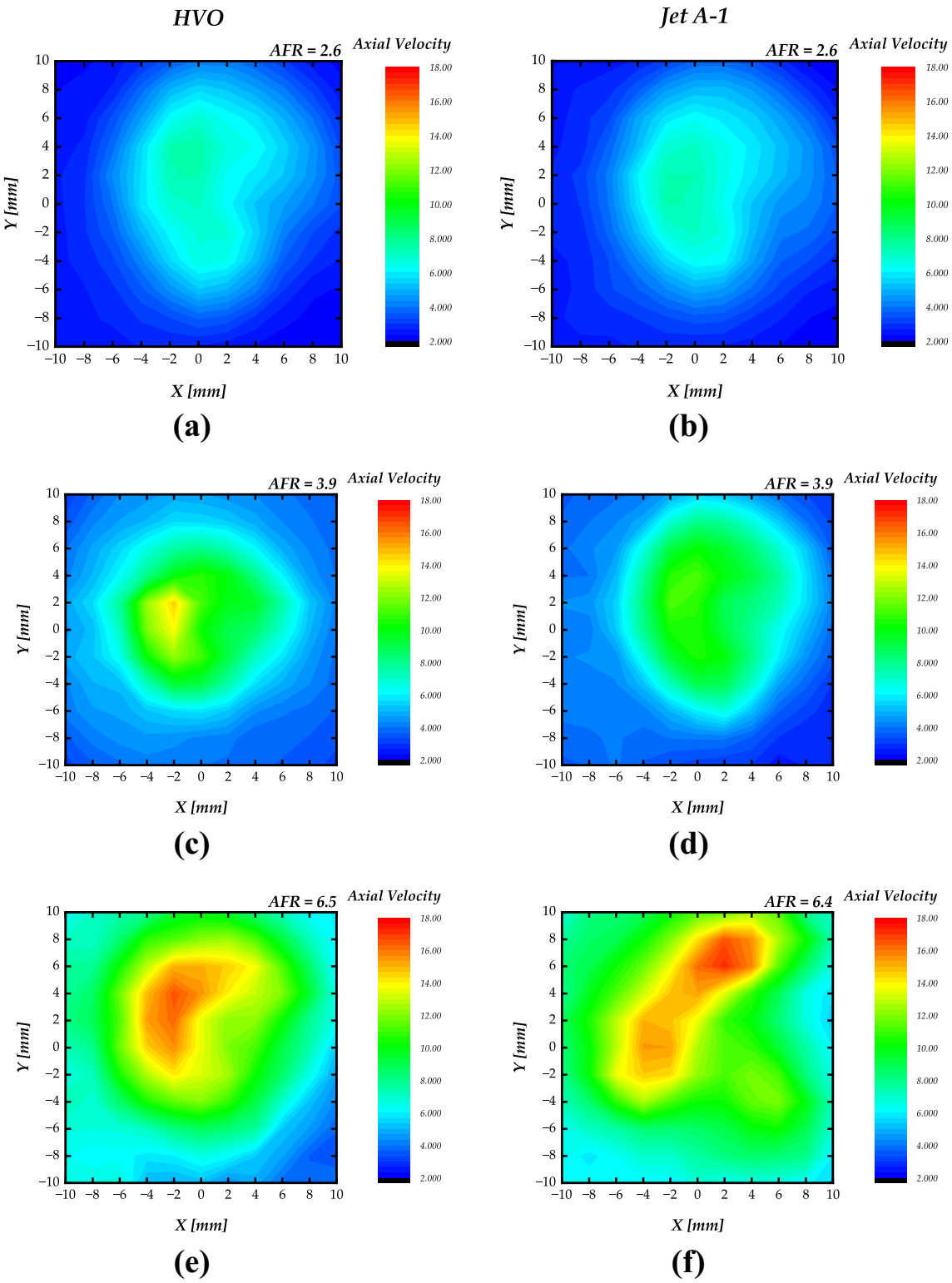

Fig. 23 Contour of the axial velocity (m/s) for X and Y radial distances for HVO: **a** AFR = 2.6; **c** AFR = 3.9; **e** AFR = 6.5. For Jet A-1: **b** AFR = 2.6; **d** AFR = 3.9; **f** AFR = 6.4

discrete distributions. However, in these tests, if the null hypothesis should not be rejected for two continuous functions, how does one know which function best describes the measured results? In the KS method, the function with the minimum value of the maximum deviation observed between the discrete and continuous is decided as the one that best describes the data. However, Fig. 24 shows a case where the Log-Normal surpassed the Gamma PDF by a marginal value (see magnification in the plot), implying that the KS test indicates the Log-Normal as the best PDF that describes drop sizes, failing to capture how it fails to capture the distribution behavior for sizes smaller than 5 μm.

Therefore, KS test methods are unable to capture the nature of the mathematical probability distribution function underlying the sizes resulting from liquid atomization. Therefore, in this study, a method based on information theory using the differential informature defined in Sect. 3 was introduced and explored. If one analyzes each measurement point to compare the differential informature retrieved from data ($H_{\Delta,e}$) with the analytical differential informature ($H_{\delta,e}$) of the best adjustment of each mathematical function in Table 6, both Log-Normal and Gamma distribution functions appear in the grid as the ones that best describe the measured drop size distributions.

The Weibull does not produce any best adjustment. Although a local exhaustive analysis is beyond the scope of the present work, by increasing the AFR and the spray propagation plane Z, the dominant distribution describing all points in the measurement plane tends to be Gamma. Therefore, all drop size data measured in a plane were accumulated into a single sample to express the spray crossing a plane as an event. Table 6 also includes the analytical solution for the *differential informature* (Michalowicz and Nichols 2013), where $\psi(x)$ is the digamma function and γ represents the Euler–Mascheroni constant. The reasoning behind the *differential informature* is the comparison of the value obtained from the discrete drop

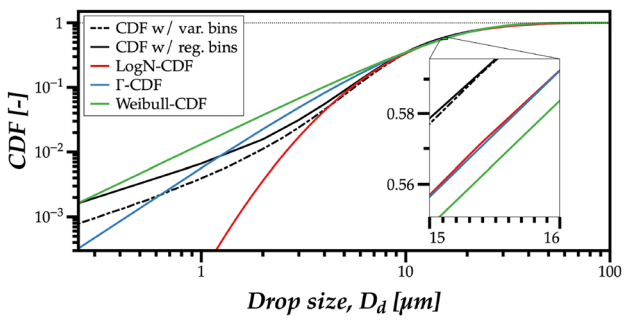

Fig. 24 Example of the cumulative distribution function (CDF) with regular and variable bin sizes compared to the Log-Normal, Gamma, and Weibull that best fitted the entire spray of HVO with AFR = 6.56 at $Z = 10$ mm

Table 6 Drop size mathematical distribution used to fit discrete histograms in spray science

Type	Function, $p(d)$	$H_{\delta,e}$
Log-Normal	$\frac{1}{\sqrt{2\pi}sD_{50}}\exp\left(-\frac{\ln(d/D_{50})^2}{2s^2}\right)$	$\frac{1}{2}\ln\left(2\pi e s^2 D_{50}^2\right)$
Gamma	$\frac{d^{a-1}}{b^a\Gamma(a)}\exp\left(-\frac{d}{b}\right)$	$\ln(b\Gamma(a)) + (1-a)\psi(a) + a$
Weibull	$\frac{b}{a}\left(\frac{d}{a}\right)^{b-1}\exp\left(-\left(\frac{d}{a}\right)^b\right)$	$\ln(a/b) + ((a-1)/a)\gamma + 1$

size distribution with the analytical value obtained for the three continuous mathematical functions considered. The best mathematical distribution function describing the discrete probability distribution is that with the minimum difference between these values.

Figure 25 depicts the ratio between the discrete *differential informature* ($H_{\Delta,e}$) and analytical value ($H_{\delta,e}$) for the three distribution mathematical functions considered. Each data point contained data for the entire measurement plane. In general, with both fuels, the Gamma distribution function best describes the drop sizes formed in this air-assisted swirl atomizer. Above a differential *informature* of 4 *nats*, both the Log-Normal and Gamma distribution functions produce similar fittings.

Recently, Cejpek et al. (2023) argued in favor of a Log-Normal distribution using the visual similarity between discrete and continuous drop size distributions. Earlier, Tratnig and Brenn (2010) argued in favor of the Gamma distribution, modifying it by empirically adding a second exponential term to cover the larger drop sizes present in the spray. However, the authors evaluated similarity using moments of the distribution, which is not an accurate strategy (Panão and Moreira 2008). Later, Dumouchel (2006) used the maximum entropy formalism (a designation we disagree with for the reasons discussed in Sect. 3) and obtained a Gamma distribution. Although the conclusions of Cejpek et al. (2023) and Tratnig and Brenn (2010) seem contradictory, the fact that the latter authors added an exponential term to their Gamma distribution function points to the hypothesis that the actual distribution function could be a weighted average of two physical effects: 1) the exponential growth process of drop size diversity leading to a Log-Normal, as explained in Panão (2023); 2) the liquid temporal fragmentation leading to a Gamma distribution function. However, the research hypothesis suggested by the infodynamic analysis will be the subject of future work. Henceforth, because the Gamma PDF is the dominant one from the differential informature point of view, we consider it in the comparative infodynamic analysis of the two fuels.

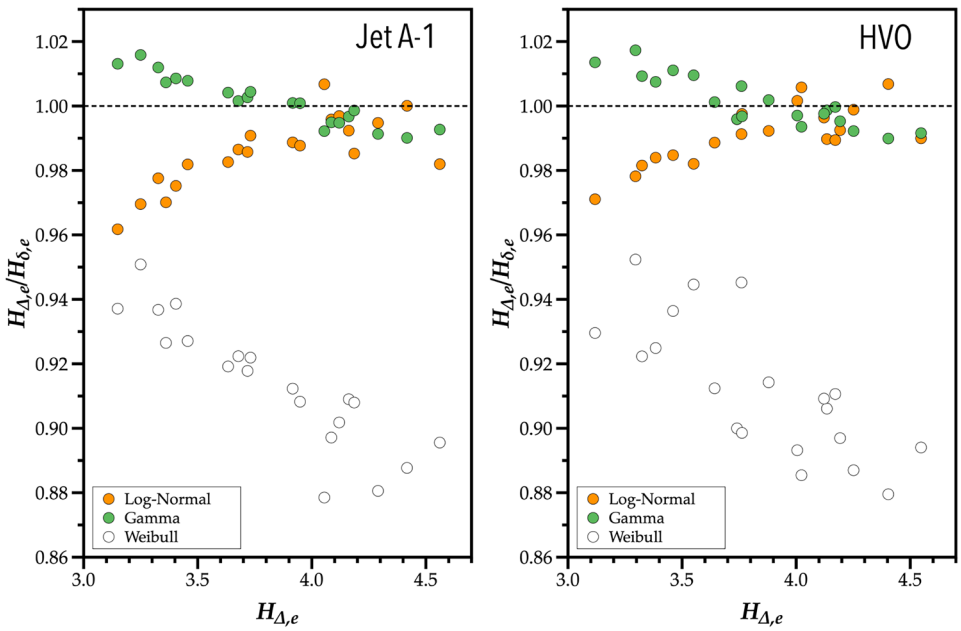

Fig. 25 Comparison between the discrete and analytical differential informature based on drop size. The Log-Normal is best in 80% of the cases, but only in one case is this difference significant

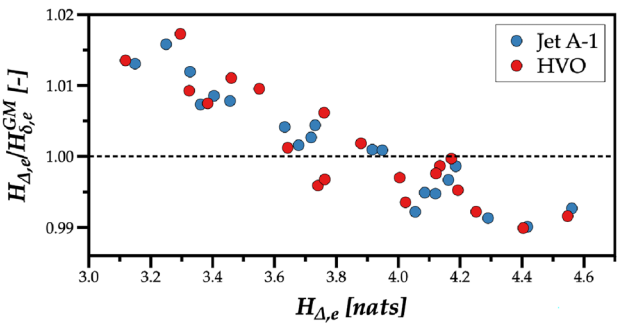

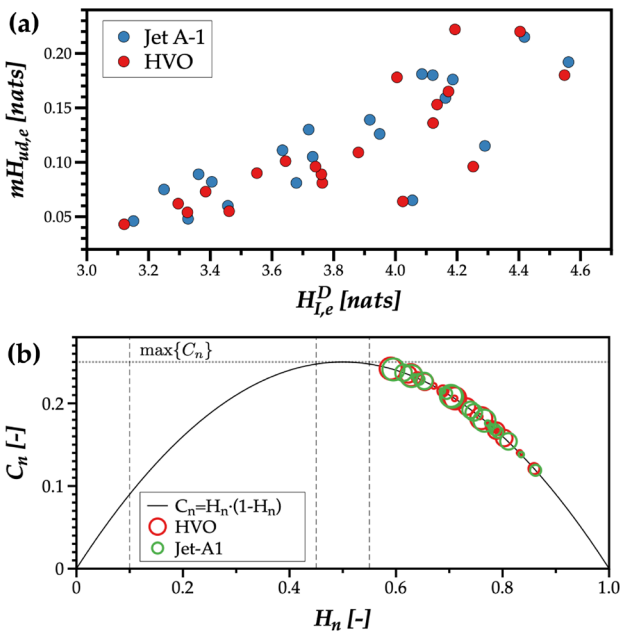

Fig. 26 Comparison of the ratios between the discrete and analytical differential informatures and the discrete differential informatures of Jet A-1 and HVO

Fig. 27 Relation between **a** the mutual informature ($mH_{ud,e}$) for both fuels and the several operating conditions and measurement planes, and **b** the corresponding results of the spray statistical complexity with symbols' size proportional to the Z distance

Figure 26 compares the ratios between the discrete and analytical differential informatures for both fuels as a function of the discrete value. The plot shows the informational similarity of the sprays produced with different fuels and a ±2% marginal difference when adjusting a Gamma distribution function to the experimental values, validating the dominant nature of liquid atomization associated with the temporal event of ligament fragmentation.

In terms of mutual informature, Eq. (16), Fig. 27 shows a proportional relation with the drop size informature and similar for both fuels. A large drop size informature indicates a higher variability of drop sizes, and a high mutual informature means that a higher amount of information on drop size is shared with the information on drop velocity. However, it is noteworthy that $mH_{ud,e}$ is one order of magnitude lower than $H^D_{I,e}$, meaning there is a low level of information of the velocity contained in drop size. This infodynamic result is consistent with the Independence of the spatial distributions between droplet size and velocity discussed in Sect. 4.4. As shown in Fig. 7, the lower levels of informature are in the center of the spray planar pattern, and globally, uniformity of informature occurs as the spray develops in its propagation path (Z-direction). This uniformity of the spray spatial information, while it develops, appears to be correlated with

the trend of increasing complexity, as shown in Fig. 27b associating the symbol size to the measurement plane distance from the nozzle. Although not included in this study, the spray complexity maps tended toward a uniform distribution with Z and AFR.

To understand how the fuel or air flowrates produce changes in spray information, Fig. 28 considers both fuels and shows consistent results for the evolution of spray complexity toward a higher balance between variability and structure. The organization levels as the spray develops and propagates in the Z-direction depend on the droplet formation and dispersion in the environment. A larger air mass flowrate means that aerodynamic forces begin to dominate liquid atomization, lowering the amount of information in the spray. Therefore, for a low fuel mass flowrate, Fig. 28 shows a significant increase in spray complexity when duplicating the air mass flowrate. The same change occurred when maintaining the air mass flowrate and duplicating the fuel mass flowrate, as shown in Fig. 28b.

The purpose of this work is to use an infodynamic analysis to compare a conventional fuel (Jet A-1) with an alternative fuel (HVO). Thus far, the results presented point to the production of similar sprays. Therefore, for a higher fuel mass flowrate ($\dot{m}_f$ =< *spanclass =′ convertEndash′* > 0.08 – 0.09 < */span* > $[g/s]$) and varying the air mass flowrate, one would expect similar complexity maps for the aerodynamic effect on the spray complexity while it propagates. However, Fig. 29 shows some differences between the fuels. Specifically, with HVO, aerodynamic forces produce a different initial complexity condition, but the Z = 10 mm plane represents a common transition of a similar amount of complexity, above which the spray seems to evolve in the sense of returning to the initial condition until Z = 15 mm. After this plane, the evolution of spray complexity followed a similar informational pattern until Z = 20 mm. These results suggest that the sprays of both fuels are similar, only after 15 mm below the injector nozzle. In addition, if one assumes the principle of evolution of physical systems toward higher levels of complexity, as observed in the natural world, this spray direction requires a higher dominance of aerodynamic forces and a minimum development distance.

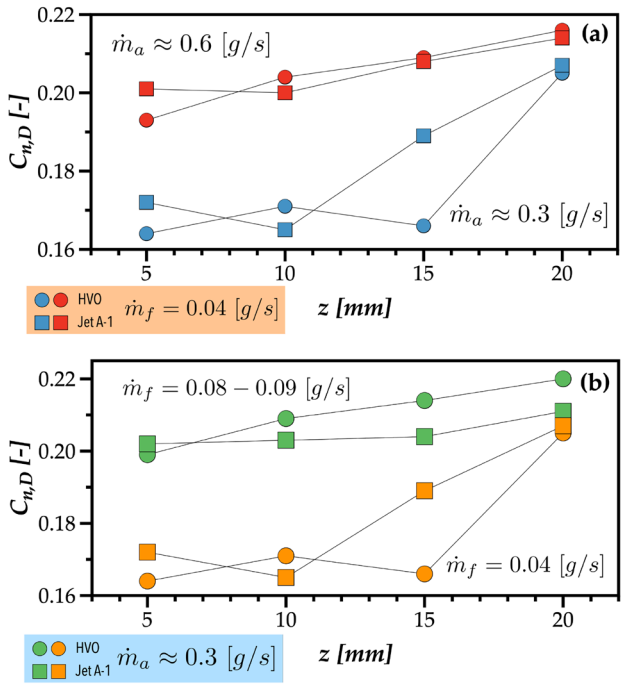

Fig. 28 Evolution of the spray complexity **a** for a constant mass flowrate and varying air flowrate and **b** similar air flowrates and different mass flowrates

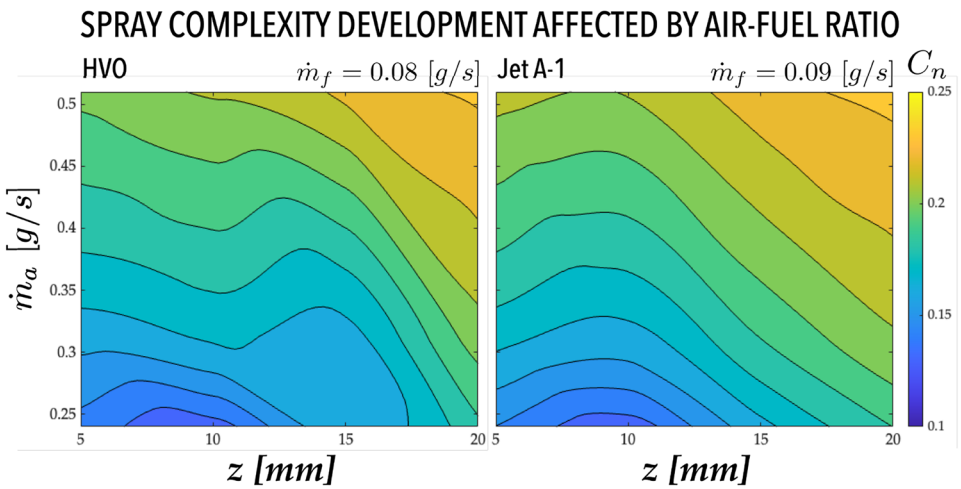

Fig. 29 Comparison between HVO and Jet A-1 in terms of the spray complexity

The analysis of the spray complexity as a function of AFR is shown in Fig. 30. The complexity is described by the function:

$$C_n = 0.24[1 - exp(-0.38 \cdot AFR)] \tag{20}$$

This equation captures the overall behavior of the spray complexity with the increase of AFR. The result shows that for lower AFR, the complexity increases sharply to a critical value, beyond which diminishing returns are observed. To determine the point from which diminishing returns are considered, the following expression is adopted:

$$\left|\frac{dC_n}{dAFR}\right| = 0.01 \tag{21}$$

The spray complexity exhibits diminishing returns beyond AFR = 5.74 as C_n approaches a plateau. This means that increasing AFR above this value no longer induces significant changes in spray complexity. Moreover, a notable transition in spray behavior occurs at AFR ≈ 8.2, highlighting the dominance of aerodynamic forces in liquid atomization. To find this transition peak on the spray complexity, $f(AFR)$ is subtracted from the C_n. This analysis shows that the spray may experience large liquid structures or ligaments fragment into smaller droplets for low AFR. As AFR increases, secondary atomization may dominate, leading to finer atomization and a more complex spray structure. Similar findings were previously discussed Lorenzetto and Lefebvre (1977); Rizkalla and Lefebvre (1975) indicating limited improvement in the atomization is gained by raising the AFR above a value of around five. The results provide insight into optimizing the operating conditions for improved spray atomization in air-assisted atomizers.

The following section presents a new approach for spray characterization that focuses on droplets as information carriers. With the advent of artificial intelligence, a synthesis

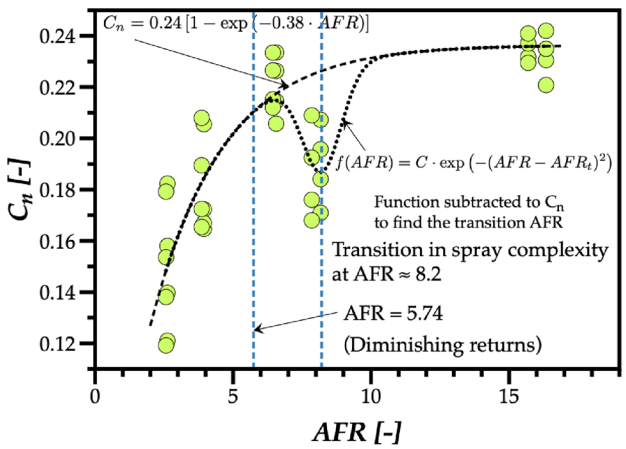

Fig. 30 Spray complexity (C_n) as a function of the AFR

between thermofluid engineering and information theory is needed if one aspires to produce intelligent systems capable of adapting their operating conditions to achieve the best performance. In addition, although providing data on average sizes, velocity distributions, and spray angles is helpful for combustion chamber design, these parameters might not capture the complexity and diversity of the spray dynamic characteristics. An example of the insights of information theory into spray characterization lies in quantifying the drop size diversity of the spray. Panão et al. (2020) showed how the normalized *informature* (although designated in the paper as Shannon entropy), H_n, combined with the standard deviation of a volume-weighted drop size distribution, SD_v, allows distinguishing the polydispersion and heterogeneity degrees of drop size diversity, respectively. However, while *informature* is proportional to the amount of information required owing to the diversity of drop sizes, its formulation lacks context. The following section considers the implications of this approach for the meaning of concepts such as entropy and explores a conceptual framework to add context to spray indeterminacy. The expectation is to develop new characterization methods when using laser diagnostic techniques as *infosensors* and improve our understanding of spray dynamics from the perspective of changes captured by information flows.

4.6 Spray infodynamics

According to Grunwald (2005), *infodynamics* captures the dynamics of information in its transformation into knowledge by intelligent agents. A system is *intelligent* if it follows a cycle of perception, reasoning, feedback, and knowledge updates. In spray infodynamics, droplets are objects containing spray knowledge (size and velocity characteristics). Information flows through the spray propagation path through these droplets as objects, and interaction events with the surrounding environment change the conveyed information. A Phase-Doppler Interferometer is a communication channel that interfaces with the processing unit and software as agents that provide access to the object's knowledge (perception) to understand it (reasoning). With this understanding, one can adjust the operating conditions if needed (feedback), leading to a knowledge update expressed by droplets (objects) with altered characteristics.

The *informature* $H_{1,b}$ quantifies the amount of information required to describe a parameter without context because it depends solely on the probability distribution. The higher this parameter is, the more droplets of different sizes that are relevant to describe the spray. The opposite would mean that the droplets have a dominant single size in the spray, as produced by a monosize injector.

Shannon (1948) described the term introduced here in Eq. (10), H_b, as a measure of uncertainty but later decided

to designate it as *entropy*. The Gibbs and Boltzmann entropies are particular cases of H_b, with Boltzmann introducing the constant bearing his name (k_B) to maintain the units of the original concept by Clausius. Later, Gibbs obtained a general form for thermodynamic entropy, considering that microstates could have different probabilities of occurrence. Based on Clausius's intuition that entropy is related to the transformation occurring in a system Sect. 3 introduced the concept of *infotropy* as a *contextualized measure of information*. For example, in the context of thermodynamics, the corresponding parameter K_c in Eq. (10) is the Boltzmann constant k_B. We apply the *infotropy* concept within the spray science context, comparing the two fuels under research, to understand how information flows in the liquid atomization process.

Consider K_c as a spray contextual scale parameter affected by the non-deterministic nature of the liquid atomization process. The *infotropy*, defined as the contextual transformation of a spray characteristic, is a combination of context (K_c) and indeterminacy ($H_{I,b}$), as defined in Eq. (10), $H_b = K_c \cdot H_{I,b}$. If the variation of H_b generates an *infodynamic flow*, it implies that

$$dH_b = dK_c H_{I,b} + K_c dH_{I,b} \tag{22}$$

where dK_c represents a change in context and $dH_{I,b}$ represents a change in the degree of indeterminacy.

Assuming as a diffusive approximation that the sensibility of the infotropy to its context is

$$\frac{dH_b}{dK_c} = \kappa \tag{23}$$

with κ constant. Applying Eq. (23) in (22) and integrating the outcome between a reference and a subsequent event (in space or time), one could determine the constant κ as

$$\kappa = \frac{\left(K_c/K_{c,0}\right)H_{I,b} - H_{I,b,0}}{K_c/K_{c,0} - 1} \tag{24}$$

where $K_{c,0}$ and $H_{I,b,0}$ are the scale context and the *informature* of the reference event. Using the plane at Z = 5 mm as the reference event and planes Z = 10, 15, 20 mm as subsequent events through which information flows, one can determine, in principle, the value of κ.

Several contexts are considered: 1) the aforementioned heterogeneity degree of drop size diversity, SD_v; 2) the Sauter mean diameter, *SMD*, because it is a physical measure related to the atomization efficiency (Panão 2022); and 3) the Weber number due to its essential role in drop formation and its association with the classification of atomization regimes. The contextual ground for the scale parameter K_c that fulfilled the assumption in Eq. (23) is the Weber number.

The median Weber number ($K_c = \mathrm{We}_{d50}$) was obtained from the discrete distribution of Weber for each measurement plane considering variable size classes because of the changes in the order of magnitude of the droplet Weber number ($\mathrm{We}_d = \rho u_d^2 d/\sigma$). For the Jet A-1, $\kappa = 3.94 \pm 5.1\%$ and for HVO, $\kappa = 4.06 \pm 6.6\%$ using Eq. (24). However, for both fuels (Jet A-1 and HVO), Fig. 31 depicts the linear relationship between the infotropy and contextual parameter (Weber in this case). From the linear fitting, it is noteworthy that the sensitivity of the infodynamic infotropy with the Weber as context results in $dH_e/d\,\mathrm{We}_{d50} = 3.6$ with $R^2 = 0.997$, which is similar to the previous values obtained by analyzing the information flow for each fuel between events/planes.

The similar sensitivity of infotropy to its context in both fuels indicates that the liquid atomization process affects the spray's ability to transport information more than the differences in the properties of the fluid. The similarity between the drop size distributions explored in the previous section and the similarity of the information flows allows us to hypothesize that the differences in the dynamic viscosity (see Table 3) are irrelevant in this liquid atomization strategy. A possible reason could be the dominant effect of aerodynamic mechanisms in the swirl fluidic structure on spray formation, as observed from the complexity point of view in the previous section. Therefore, the infodynamic comparative analysis suggests that considering HVO as an alternative fuel in aviation might depend on choosing the appropriate atomization strategy that makes the effects of the parameters with the more prominent differences meaningless.

5 Conclusions

After the 28th Conference of Parties (COP28), the urgency of transitioning from fossil fuels to more sustainable alternatives is underscored. This research focuses on evaluating biofuels, explicitly focusing on hydroprocessed vegetable oil (HVO) as a potential substitute for conventional

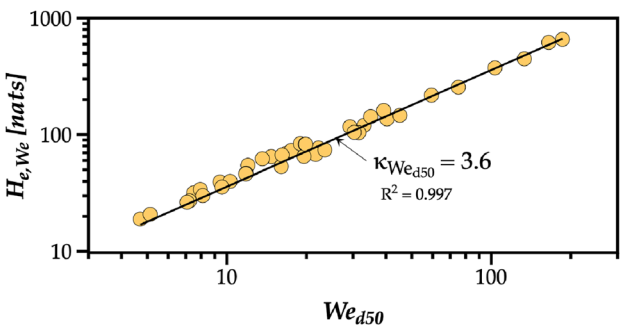

Fig. 31 Relation between the infotropy of the Weber number for both fuels (Jet A-1 and HVO), showing the linear variation assumed in Eq. (24)

aviation fuels, such as Jet A-1. Central to our analysis is understanding the primary atomization and comparing droplet sizes in fuel sprays, which is a parameter critical to optimizing the combustion process. If the atomization process becomes more efficient, it reduces the fuel emissions related to the droplet sizes in a spray. In light of this, decarbonization is a relevant topic because introducing sustainable aviation fuels is imperative to mitigate environmental concerns. Will the sprays produced by alternative aviation fuels work on injectors optimized for conventional fuels?

From the analysis of the breakup length, regardless of the fuel, increasing the momentum flux leads to a reduction in the normalized mean breakup length, where Jet A-1 possesses a slightly lower breakup length. Additionally, an empirical correlation based on the experimental data is provided, being in good agreement with the literature. This correlation indicates that the normalized mean breakup length exhibits a power law relation with the momentum flux ratio. Considering the infodynamic analysis, a transition is detected in M = 14, highlighting the relevance of the air in the atomization process. In the downstream nozzle, regardless of the fuel employed, an increase in the AFR reduces the SMD in both the radial and axial axes. Despite the AFR considered, the larger droplet diameters are presented mainly on the periphery of the spray, whereas the lower SMD was observed in the central region. The similar spray behaviors of Jet A-1 and HVO are clearly perceptible at larger AFRs.

Moreover, to answer the above question, the principles of information theory are integrated into spray science, introducing the appropriate terminology of *informature* (and differential informature) that quantifies the amount of information in a physical system with a non-deterministic nature, *infotropy* as a contextualized informature, and *infosensor* as the Phase-Doppler Interferometer that captures the non-deterministic nature of the physical system. These concepts are innovatively applied to analyze and compare discrete and continuous probability distributions of droplet sizes by employing differential information as the cornerstone of this analysis. Our findings reveal a striking similarity between the drop size distributions of HVO and the traditional Jet A-1 fuel. Notably, although the Gamma mathematical function accurately characterizes the drop size distribution in swirling sprays, the Log-Normal presented similar results to Gamma, indicating that liquid atomization could hybrid a temporal fragmentation of ligaments and an exponential growth pattern in drop size diversity. We also evaluated the spray complexity and showed that both fuels produced spray evolving toward higher complexity states, balancing the variability of drop sizes and order imbued in the interactive atomization mechanism between the fuel and air flows. However, from the viewpoint of spray complexity, the similarity between the sprays requires the dominance of aerodynamic forces in liquid atomization, evidencing its influence in the transition defined in $C_n = 8.2$ and a minimum development distance.

Finally, we propose a novel lexicon for spray characterization, *infodynamics*, which conceptualizes a spray as a network of information flows between droplets and their interactive events. The *infotropy* concept provides context-rich insights into spray dynamics. In this study, we searched for a contextual scale that expressed a constant sensitivity of infotropy to its context. From several relevant parameters characterizing a spray, the contextual scale based on the Weber number is aligned with the constant sensibility assumption. This means that spatial variations in the context generated by the interaction events in the atomization process produce linear variations in the infodynamic transformation of the physical system expressed by its infotropy.

Our exploration endorses HVO as a viable alternative to traditional aviation fuels by analyzing primary and secondary atomization, especially from the perspective of spray infodynamics. In addition, our informational approach to spray characterization is novel and intends to encourage new insights by introducing an informational perspective, enabling future research to better capture the inherent degree of transformation within sprays, inherently linked to their indeterminate nature. Ultimately, this approach facilitates the quantification of complexity in spray phenomena, moving beyond qualitative descriptions toward a robust, quantitative understanding.

Acknowledgements Inês A. S. Ferrão acknowledges Fundação para a Ciência e Tecnologia (FCT), Portugal for the provision of PhD scholarship with the reference SFRH/BD/144688/2019. The authors would like to acknowledge the Fundação para a Ciência e Tecnologia (FCT) for partially financing the research through projects PTDC/EMETED/7801/2020 and UIPD/50022/2020 (DOI: 10.54499/UIDP/50022/2020) and UIDB/50022/2020 (DOI: 10.54499/UIDB/50022/2020) and 10.54499/LA/P/0079/2020. Ana S. Moita also acknowledges FCT for partially financing her contract through EECINST/00043/2021/CP2797/CT0005, (DOI: 10.54499/CEECINST/00043/2021/CP2797/CT0005).

Author Contributions Inês A. S. Ferrão contributed to conceptualization, methodology, validation, formal analysis, investigation, data curation, and writing—original draft, and provided software. Miguel R. O. Panão was involved in conceptualization, methodology, validation, formal analysis, investigation, data curation, resources, writing—original draft, and project administration and provided software. Miguel A. A. Mendes contributed to resources, writing—review and editing, visualization, supervision, funding acquisition, and project administration. Ana S. H. O. Moita was involved in resources, writing—review and editing, visualization, supervision, funding acquisition, and project administration. André R. R. Silva contributed to resources, writing—review and editing, visualization, supervision, funding acquisition, and project administration.

Funding Open access funding provided by FCT|FCCN (b-on).

Data Availability No datasets were generated or analyzed during the current study.

Declarations

Conflict of interest The authors declare no conflict of interest.

Open Access This article is licensed under a Creative Commons Attribution 4.0 International License, which permits use, sharing, adaptation, distribution and reproduction in any medium or format, as long as you give appropriate credit to the original author(s) and the source, provide a link to the Creative Commons licence, and indicate if changes were made. The images or other third party material in this article are included in the article's Creative Commons licence, unless indicated otherwise in a credit line to the material. If material is not included in the article's Creative Commons licence and your intended use is not permitted by statutory regulation or exceeds the permitted use, you will need to obtain permission directly from the copyright holder. To view a copy of this licence, visit http://creativecommons.org/licenses/by/4.0/.

References

Abrantes I, Ferreira AF, Silva A, Costa M (2021) Sustainable aviation fuels and imminent technologies - co2 emissions evolution towards 2050. J Clean Prod 313:127937

Aatola H, Larmi M, Sarjovaara T (2008) Hydrotreated vegetable oil (hvo) as a renewable diesel fuel: trade-off between nox, particulate emission, and fuel consumption of a heavy duty engine. SAE Int J Engines. https://doi.org/10.4271/2008-01-2500

Afonso F, Sohst M, Diogo CM, Rodrigues SS, Ferreira A, Ribeiro I, Marques R, Rego FF, Sohouli A, Portugal-Pereira J et al (2023) Strategies towards a more sustainable aviation: a systematic review. Prog Aerosp Sci 137:100878

Beck J, Lefebvre A, Koblish T (1991) Airblast atomization at conditions of low air velocity. J Propul Power 7(2):207–212

Blakey S, Rye L, Wilson CW (2011) Aviation gas turbine alternative fuels: a review. Proc Combust Inst 33(2):2863–2885

Chuck CJ, Donnelly J (2014) The compatibility of potential bioderived fuels with jet a-1 aviation kerosene. Appl Energy. https://doi.org/10.1016/j.apenergy.2013.12.019

Cabrera E, Sousa JMM (2022) Use of sustainable fuels in aviation-a review. Energies 15(7):2440

Chong CT, Hochgreb S (2015) Effect of atomizing air flow on spray atomization of an internal-mix twin-fluid atomizer. Atomization and Sprays **25**(8)

Chigier N (1996) Regimes of jet breakup and breakup mechanisms (physical aspects). Prog Astronaut Aeronaut 166:109–134

Cejpek O, Maly M, Prinz F, Hajek O, Jedelsky J, Jicha M (2023) Adaptation of conical liquid sheet and spray morphologies to cross-flowing gas. Int J Multiph Flow 172:104714

Dunand A, Carreau J-L, Roger F (2005) Liquid jet breakup and atomization by annular swirling gas jet. Atomization sprays 15(2)

Denbigh K (1981) How subjective is entropy? Chem Br 17:168

Dumouchel C (2006) A new formulation of the maximum entropy formalism to model liquid spray drop-size distribution. Part Part Syst Charact 23(6):468–479

Dumouchel C (2008) On the experimental investigation on primary atomization of liquid streams. Exp Fluids 45:371–422

Eroglu H, Chigier N, Farago Z (1991) Coaxial atomizer liquid intact lengths. Phys Fluids A 3(2):303–308

Ershov MA, Savelenko VD, Burov NO, Makhova UA, Mukhina DY, Aleksanyan DR, Kapustin VM, Lobashova MM, Sereda AV, Abdellatief TM et al (2023) An incorporating innovation and new interactive technology into obtaining sustainable aviation fuels. Energy 280:128156

Esposito MC (2019) Analysis of primary atomization in sprays using direct numerical simulation. PhD thesis, Universitat Politècnica de València

Feldman DP, Crutchfield JP (1998) Measures of statistical complexity: why? Phys Lett A 238(4–5):244–252

Ferrão I, Mendes M, Moita A, Silva A (2024) Insights on liquid jet breakup and spray formation of an air-assisted atomizer: Conventional and alternative jet fuel. In: 21st International Symposium on Applications of Laser and Imaging Techniques to Fluid Mechanics, Lisbon, Portugal

Ferrao IA, Silva AR, Moita AS, Mendes MA, Costa MM (2021) Combustion characteristics of a single droplet of hydroprocessed vegetable oil blended with aluminum nanoparticles in a drop tube furnace. Fuel 302:121160

Grunwald S (2005) Infodynamics: how to maximize the efficiency of intelligent agents. Xlibris Corporation, Bloomington

Hopfinger E, Lasheras JC (1994) Breakup of a water jet in high velocity co-flowing air. In: ICLASS 94 proceedings of the sixth international conference on liquid atomization and spray systems. Begell House

Inc TM (2022) MATLAB Version: 9.13.0. https://www.mathworks.com

Kumar M, Karmakar S, Kumar S, Basu S (2021) Experimental investigation on spray characteristics of jet a-1 and alternative aviation fuels. Int J Spray Combust Dyn 13(1–2):54–71

Khan MZA, Khan HA, Ravi SS, Turner JW, Aziz M (2023) Potential of clean liquid fuels in decarbonizing transportation-an overlooked net-zero pathway? Renew Sustain Energy Rev 183:113483

Kumar A, Sahu S (2018) Liquid jet breakup unsteadiness in a coaxial air-blast atomizer. Int J Spray Combust Dyn 10(3):211–230

Kumar A, Sahu S (2019) Large scale instabilities in coaxial air-water jets with annular air swirl. Phys Fluids 31(12)

Khan N, Sudhakar K, Mamat R (2021) Role of biofuels in energy transition, green economy and carbon neutrality. Sustainability 13(22):12374

Leroux B, Delabroy O, Lacas F (2007) Experimental study of coaxial atomizers scaling. part i: dense core zone. Atomization Sprays 17(5)

Lefebvre AH (1980) Airblast atomization. Prog Energy Combust Sci 6(3):233–261

Lefebvre A (1992) Energy considerations in twin-fluid atomization. J Eng Gas Turbines Power

Lasheras JC, Hopfinger E (2000) Liquid jet instability and atomization in a coaxial gas stream. Annu Rev Fluid Mech 32(1):275–308

Lorenzetto G, Lefebvre AH (1977) Measurements of drop size on a plain-jet airblast atomizer. AIAA J 15(7):1006–1010

Lefebvre AH, McDonell VG (2017) Atomization and sprays. CRC Press, Boca Raton

Lin SP, Reitz RD (1998) Drop and spray formation from a liquid jet. Annu Rev Fluid Mech 30(1):85–105

Miesse C (1955) Correlation of experimental data on the disintegration of liquid jets. Ind Eng Chem 47(9):1690–1701

Michalowicz JV, Nichols JM, Bucholtz F (2013) Handbook of differential entropy. CRC Press, New York

Mao C-P, Oechsle V, Chigier N (1987) Drop size distribution and air velocity measurements in air assist swirl atomizer sprays. J Fluids Eng 109(1):64–69

Mikkonen S, Honkanen M, Kuronen M (2013) HVO, hydrotreated vegetable oil. A premium renewable biofuel for diesel engines. https://www.osti.gov/etdeweb/biblio/22114203

Okolie JA, Awotoye D, Tabat ME, Okoye PU, Epelle EI, Ogbaga CC, Güleç F, Oboirien B (2023) Multi criteria decision analysis for the evaluation and screening of sustainable aviation fuel production pathways. Iscience

Panão MRO (2012) Assessment of measurement efficiency in laser-and phase-doppler techniques: an information theory approach. Meas Sci Technol 23(12):125304
Panão M (2022) Ultrasonic atomization: new spray characterization approaches. Fluids 7(1):29
Panão M (2023) Why drop size distributions in sprays fit the lognormal. Phys Fluids 35(1)
Panão MR (2025) On the infodynamics of ramifications in constructal design. Biosystems 248:105388
Pinto G, Costa R, Souza T, Rosa A, Raats O, Roque L, Frez G, Coronado C (2023) Experimental investigation of performance and emissions of a ci engine operating with hvo and farnesane in dual-fuel mode with natural gas and biogas. Energy 277:127648
Panão M, Moreira A (2008) A real-time assessment of measurement uncertainty in the experimental characterization of sprays. Meas Sci Technol 19(9):095402
Panão MO, Moita AS, Moreira AL (2020) On the statistical characterization of sprays. Appl Sci 10(17):6122
Payri R, Salvador FJ, Gimeno J, Morena J (2011) Analysis of diesel spray atomization by means of a near-nozzle field visualization technique. Atomization Sprays 21(9)
Reitz R, Bracco F (1982) Mechanism of atomization of a liquid jet. Phys Fluids 25(10):1730–1742
Rizkalla A, Lefebvre AH (1975) The influence of air and liquid properties on airblast atomization
Roudini M, Wozniak G (2018) Experimental investigation of spray characteristics of pre-filming air-blast atomizers. J Appl Fluid Mech 11(6):1455–1469
Shannon CE (1948) A mathematical theory of communication. Bell Syst Tech J 27(3):379–423
Soni SK, Kolhe PS (2021) Liquid jet breakup and spray formation with annular swirl air. Int J Multiph Flow 134:103474
Scott M, Lindsey R (2016) Which emits more carbon dioxide: volcanoes or human activities. June, Vol 15
Stone JV (2015) Information Theory: a Tutorial Introduction. Sebtel Press, Montgomery
Sikka R, Vågsæther K, Bjerketvedt D, Lundberg J (2021) Experimental study of primary atomization characteristics of sonic air-assist atomizers. Appl Sci 11(21):10444
Shannon CE (1949) Weaver, W: The Mathematical Theory of Communication, by CE Shannon (and Recent Contributions to the Mathematical Theory of Communication). W. Weaver. University of Illinois Press, Champaign
Tratnig A, Brenn G (2010) Drop size spectra in sprays from pressure-swirl atomizers. Int J Multiph Flow 36(5):349–363
Tribus M, McIrvine EC (1971) Energy and information. Sci Am 225(3):179–190
Urbán A, Zaremba M, Malỳ M, Józsa V, Jedelskỳ J (2017) Droplet dynamics and size characterization of high-velocity airblast atomization. Int J Multiph Flow 95:1–11
Villermaux E, Marmottant P, Duplat J (2004) Ligament-mediated spray formation. Phys Rev Lett 92(7):074501
Vijay GA, Moorthi NSV, Manivannan A (2015) Internal and external flow characteristics of swirl atomizers: a review. Atomization sprays, 25(2)
Yang M, Chen L, Wang J, Msigwa G, Osman AI, Fawzy S, Rooney DW, Yap P-S (2023) Circular economy strategies for combating climate change and other environmental issues. Environ Chem Lett 21(1):55–80
Zhao H, Liu H-F, Tian X-S, Xu J-L, Li W-F, Lin K-F (2014) Influence of atomizer exit area ratio on the breakup morphology of coaxial air and round water jets. AIChE J 60(6):2335–2345

Publisher's Note Springer Nature remains neutral with regard to jurisdictional claims in published maps and institutional affiliations.